U.S. Department of Transportation

Federal Railroad Administration

Broken Rims in Railroad Wheels

Office of Research
and Development
Washington, DC 20590

DOT/FRA/ORD-14/41

Final Report
December 2014

REPORT DOCUMENTATION PAGE

Form Approved
OMB No. 0704-0188

1. AGENCY USE ONLY (Leave blank)	2. REPORT DATE	3. REPORT TYPE AND DATES COVERED
	December 2014	Final Report, 7/2010 to 12/2012

4. TITLE AND SUBTITLE
Broken Rims in Railroad Wheels

5. FUNDING NUMBERS
Contract DTFR53-00-C-00012
Task Order 253

6. AUTHOR(S) and FRA COTR
Scott Cummings

7. PERFORMING ORGANIZATION NAME(S) AND ADDRESS(ES)
Transportation Technology Center, Inc.
55500 DOT Rd.
Pueblo, CO 81001

8. PERFORMING ORGANIZATION REPORT NUMBER

9. SPONSORING/MONITORING AGENCY NAME(S) AND ADDRESS(ES)
U.S. Department of Transportation
Federal Railroad Administration
Office of Research and Development
Washington, DC 20590

10. SPONSORING/MONITORING AGENCY REPORT NUMBER
DOT/FRA/ORD-14/41

11. SUPPLEMENTARY NOTES
COTR: John Punwani

12a. DISTRIBUTION/AVAILABILITY STATEMENT
This document is available to the public through the FRA Web site at http://www.fra.dot.gov.

12b. DISTRIBUTION CODE

13. ABSTRACT (Maximum 200 words)

Broken wheels are one of the most common types of equipment-caused train accidents. The failure of rail car wheel rims, which are usually the result of shattered rims or vertical split rims (VSR), are the leading cause of wheel-related accidents, and they are increasing as a percentage of all equipment-related accidents. The root causes of shattered rims have been agreed upon in the literature and effective mitigation procedures have already been implemented. Inspection, analysis, and testing of microcleanliness and residual stresses have increased confidence in a theory about the root cause of vertical split rim (VSR) failures in railroad wheels. However, two attempts to replicate the VSR failure mode under controlled conditions in the laboratory were unsuccessful, indicating that more research is needed to better understand VSRs and to assess the best potential mitigation methods. VSRs are thought to be the result of tread damage on the wheel surface in the form of a shell or spall that initiates cracking in the rim and produces impact loads when it comes in contact with the rail. If the crack propagates vertically to an area of tensile residual stress in the wheel rim, further crack growth is encouraged until a portion of the rim breaks free from the wheel.

14. SUBJECT TERMS
Railroad, Wheel, Crack, Rim, Broken

15. NUMBER OF PAGES
59

16. PRICE CODE

17. SECURITY CLASSIFICATION OF REPORT	18. SECURITY CLASSIFICATION OF THIS PAGE	19. SECURITY CLASSIFICATION OF ABSTRACT	20. LIMITATION OF ABSTRACT
Unclassified	Unclassified	Unclassified	

NSN 7540-01-280-5500

Standard Form 298 (Rev. 2-89)
Prescribed by ANSI Std. 239-18
298-102

METRIC/ENGLISH CONVERSION FACTORS

ENGLISH TO METRIC	METRIC TO ENGLISH
LENGTH (APPROXIMATE)	**LENGTH (APPROXIMATE)**
1 inch (in) = 2.5 centimeters (cm)	1 millimeter (mm) = 0.04 inch (in)
1 foot (ft) = 30 centimeters (cm)	1 centimeter (cm) = 0.4 inch (in)
1 yard (yd) = 0.9 meter (m)	1 meter (m) = 3.3 feet (ft)
1 mile (mi) = 1.6 kilometers (km)	1 meter (m) = 1.1 yards (yd)
	1 kilometer (km) = 0.6 mile (mi)
AREA (APPROXIMATE)	**AREA (APPROXIMATE)**
1 square inch (sq in, in^2) = 6.5 square centimeters (cm^2)	1 square centimeter (cm^2) = 0.16 square inch (sq in, in^2)
1 square foot (sq ft, ft^2) = 0.09 square meter (m^2)	1 square meter (m^2) = 1.2 square yards (sq yd, yd^2)
1 square yard (sq yd, yd^2) = 0.8 square meter (m^2)	1 square kilometer (km^2) = 0.4 square mile (sq mi, mi^2)
1 square mile (sq mi, mi^2) = 2.6 square kilometers (km^2)	10,000 square meters (m^2) = 1 hectare (ha) = 2.5 acres
1 acre = 0.4 hectare (he) = 4,000 square meters (m^2)	
MASS - WEIGHT (APPROXIMATE)	**MASS - WEIGHT (APPROXIMATE)**
1 ounce (oz) = 28 grams (gm)	1 gram (gm) = 0.036 ounce (oz)
1 pound (lb) = 0.45 kilogram (kg)	1 kilogram (kg) = 2.2 pounds (lb)
1 short ton = 2,000 pounds (lb) = 0.9 tonne (t)	1 tonne (t) = 1,000 kilograms (kg)
	= 1.1 short tons
VOLUME (APPROXIMATE)	**VOLUME (APPROXIMATE)**
1 teaspoon (tsp) = 5 milliliters (ml)	1 milliliter (ml) = 0.03 fluid ounce (fl oz)
1 tablespoon (tbsp) = 15 milliliters (ml)	1 liter (l) = 2.1 pints (pt)
1 fluid ounce (fl oz) = 30 milliliters (ml)	1 liter (l) = 1.06 quarts (qt)
1 cup (c) = 0.24 liter (l)	1 liter (l) = 0.26 gallon (gal)
1 pint (pt) = 0.47 liter (l)	
1 quart (qt) = 0.96 liter (l)	
1 gallon (gal) = 3.8 liters (l)	
1 cubic foot (cu ft, ft^3) = 0.03 cubic meter (m^3)	1 cubic meter (m^3) = 36 cubic feet (cu ft, ft^3)
1 cubic yard (cu yd, yd^3) = 0.76 cubic meter (m^3)	1 cubic meter (m^3) = 1.3 cubic yards (cu yd, yd^3)
TEMPERATURE (EXACT)	**TEMPERATURE (EXACT)**
[(x-32)(5/9)] °F = y °C	[(9/5) y + 32] °C = x °F

QUICK INCH - CENTIMETER LENGTH CONVERSION

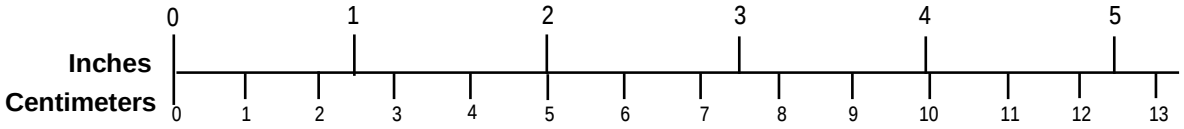

QUICK FAHRENHEIT - CELSIUS TEMPERATURE CONVERSIO

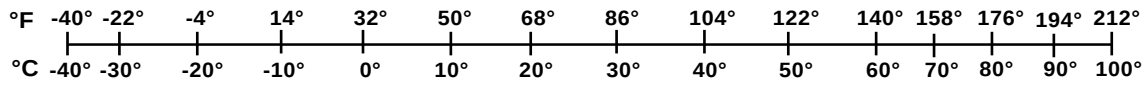

For more exact and or other conversion factors, see NIST Miscellaneous Publication 286, Units of Weights and Measures. Price $2.50 SD Catalog No. C13 10286

Updated 6/17/98

Contents

Illustrations

Tables

Executive Summary

Broken rims are the leading cause of wheel-related train accidents, and they are increasing as a percentage of all equipment-related accidents. The 3-year-average count of Federal Railroad Administration (FRA) reportable accidents attributed to broken rims has increased slightly in recent years from 16.0 (2004 to 2006) to 19.3 (2009 to 2011) (FRA 2012). Broken rim wheel failures generally fall into one of two categories: shattered rim or Vertical Split Rims (VSR).

The root causes of shattered rims have been studied and agreed upon in the literature. Effective mitigation strategies for shattered rims—for example, tighter ultrasonic testing (UT) limits on allowable defects, tighter microcleanliness limits, and the establishment of a maximum impact load criteria—have been recognized and implemented by the Association of American Railroads (AAR). Shattered rims have been on the decline for the past decade, recently accounting for less than 0.01 percent of wheel removals in the AAR car repair billing database.

Work performed by Transportation Technology Center, Inc. (TTCI) under this task order has increased confidence in a working theory about the root cause of vertical split rim (VSR) failures in railroad wheels. However, two attempts to replicate the VSR failure mode under controlled conditions in the laboratory were unsuccessful after approximately 7 million load cycles at wheel-rail loads as high as 90,000 pounds (lb), indicating that more research is needed to better understand VSRs and to assess the best potential mitigation methods.

Adding or modifying specifications for newly manufactured wheels and/or reprofiled wheels cannot be justified at this time based on the current research results. Wayside automated detection methods for cracked wheels could potentially provide some reduction in VSRs; however, many factors still need to be addressed, including the following:

- The relationship between the number of load cycles and the VSR crack size;
- The influence on this relationship of parameters such as load magnitude, impact loading, ambient temperature, and lateral position of the contact patch on the wheel tread.

VSRs are thought to be the result of tread damage on the wheel surface in the form of a shell or spall that initiates cracking in the rim and produces impact loads when it contacts the rail (Dick, et al. 2008; Lonsdale and Oliver 2011). If the crack propagates vertically into an area of tensile residual stress in the wheel rim, further crack growth is encouraged until a portion of the rim breaks free from the wheel.

Inspections of 29 VSR wheels and 6 broken flange wheels showed a broad range of wheels, including cast and forged wheels, reprofiled wheels and wheels in their first life cycle, as well as wheels removed from many different car types including cars with gross rail load ratings of 110, 100, and 70 tons. A VSR origin location was identified for each wheel. Radial depths of these origins were all found in a tight band ranging from 0.10 inch (in) to 0.25 in below the tread surface with a median value of 0.17 in. Shells were noted on the tread surface in close proximity to the origin point for 29 of the 35 wheels. Nondestructive testing revealed horizontal cracks in 27 of the 35 broken wheels and 18 of the 35 mate wheels.

Microcleanliness tests conducted on 25 VSR wheels and 5 broken flange wheels show that 28 of the 30 wheels tested met current microcleanliness standards of the Association of American Railroads (AAR). The microcleanliness of the steel in the wheels tested appears to be typical of

many wheels in service today. The residual stress patterns in the axial direction of VSR wheels and the service-worn wheels show similar trends (i.e., a large compressive residual stress near the tread surface transitioning to a large tensile residual stress at approximately 0.4-inch radial depth). This means that a crack located at the median VSR initiation depth found during inspection would only have to propagate a short distance before entering a tensile residual stress field that would accelerate the crack growth.

Two service-worn wheels with large naturally occurring subsurface horizontal cracks were cycled on a rolling load test machine at wheel-rail forces as high as 90,000 lb in an attempt to create a VSR wheel under controlled conditions. In each case, the test machine failed after approximately 7 million load cycles and the test was stopped. Neither test wheel developed a VSR crack, although post-test destructive evaluation revealed short vertical crack branches in both wheels. The horizontal cracks were found at a typical radial depth of 0.15 in, which is nearly the same radial depth as the VSR crack origins identified during the wheel inspections. Analysis showed that the cracks propagated in a transgranular fashion, indicating that material weakness was not a primary cause for the crack development in these two wheels.

Shattered rims and VSRs have some distinct differences including the following:

- Shattered rims are on the decline while accidents due to VSRs are on the rise.
- Shattered rims are reported throughout the world while VSRs are reported only in North America.
- The shattered rim failure mode is well understood by the industry and has been replicated under controlled conditions while the VSR failure mode is less well understood, and attempts to replicate this failure mode in the laboratory have not been successful.

1. Introduction

The Office of Research and Development at FRA has teamed with the AAR to fund research conducted by TTCI regarding the root cause of wheel-related accidents. This report describes research conducted to improve the understanding of the conditions necessary for broken rims on railroad wheels.

1.1 Background

Broken rim wheel failures generally fall into one of two categories: shattered rim or VSR. VSR cracks usually propagate to the front rim fillet, but can sometimes propagate to the back rim fillet resulting in a broken flange. Figure 1 shows an example of a typical VSR wheel with a crack roughly parallel to the bearing end cap, a shattered rim wheel with concentric crack growth rings roughly parallel to the tread surface, and a wheel with a VSR crack that propagated to the back rim fillet resulting in a broken flange. Much of the focus of this research will be on VSRs.

Figure 1. Typical VSR (Top Left), Shattered Rim (Top Right), and VSR Crack Resulting in a Broken Flange (Bottom)

1.2 Objectives

The purpose of the work described in this document is to identify measures for improved wheel performance by gaining a solid understanding of the root causes of broken wheel rims.

1.3 Overall Approach

The general approach used to investigate broken wheel rims includes reviewing existing data and literature, inspecting failed wheels, conducting laboratory testing, and attempting to create wheel failures under controlled conditions. The literature review and inspection of failed wheels guide the focus of the remaining approach. The laboratory testing increases our understanding of the conditions necessary to initiate the failure mode. The ability to intentionally create the VSR wheel failure mode under controlled conditions would demonstrate proper understanding of the root cause and provide opportunity to develop appropriate means of prevention.

1.4 Scope

The broken rim investigation includes a literature review, visual inspection of VSR wheels, ultrasonic hand mapping of VSR wheels, microcleanliness testing, residual stress testing, and thermal history testing. Crack growth rate tests were conducted to improve the definition of the critical stress intensity at which cracks begin to propagate. Attempts were made to produce VSR cracks on two service-worn wheels under controlled conditions.

1.5 Organization of the Report

This report is divided into sections describing the literature review, inspection, test, attempts to create broken rims under controlled conditions, current and potential future mitigation opportunities, and conclusions.

2. Literature Review

A review of existing FRA safety data, AAR car repair billing data, and relevant AAR rule changes provide an account of the past and current status of the broken wheel problem. Literature describing the efforts and findings of other research projects focused on broken wheel rims is summarized.

2.1 FRA Accident Data

The FRA safety database shows that broken wheel rims (cause code E61C "Broken rim") are a high-ranking cause of FRA reportable train accidents. A broken wheel flange (cause code E60C "Broken flange") is a much lower ranking cause of FRA reportable train accidents. The broken rim cause code includes wheels with shattered rims and wheels with VSR and does not distinguish between the failure modes. Between January 2004 and December 2011, a total of 137 accidents were attributed directly to broken rims—for an average of 17.125 broken rim accidents per year. Over this same period, 14 accidents were attributed to broken flanges. Of all equipment-related accidents, broken rim accidents are the third most common cause. Broken rims are the leading cause of wheel-related accidents (FRA 2012). Figure 2 shows the annual count of accidents attributed to broken rim and broken flange (the values for the 1970s, 1980s and 1990s are annual averages), and Figure 3 shows the broken rim and broken flange accidents as a percentage of accidents attributed to all equipment-related causes. The 3-year-average count of FRA reportable accidents attributed to broken rims has increased slightly in recent years from 16.0 (2004 to 2006) to 19.3 (2009 to 2011) (FRA 2012). The count of broken rim accidents has increased in recent years; Figure 3 shows that broken rims have not kept pace with the safety improvements seen in other accidents caused by broken flanges.

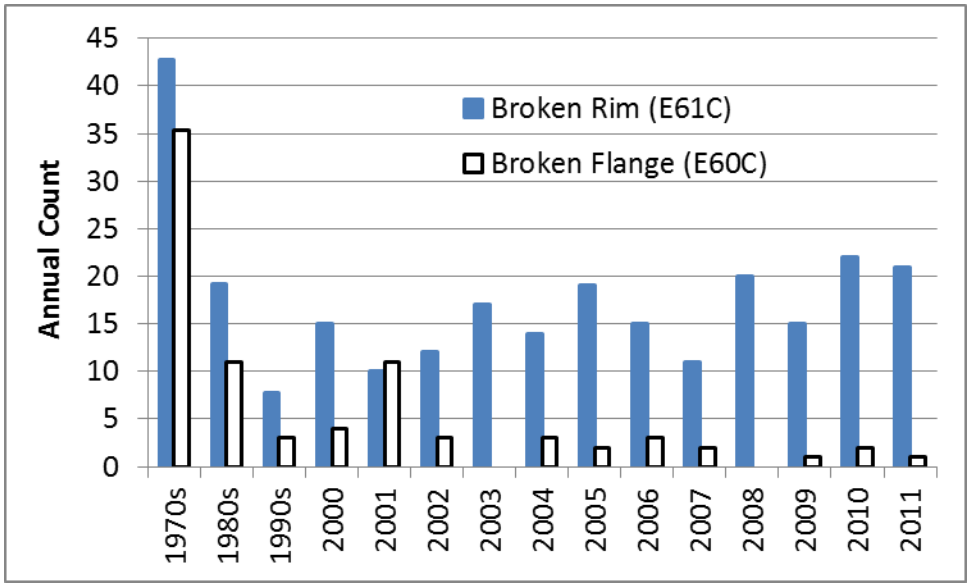

Figure 2. Broken Rim and Broken Flange Accidents from FRA Safety Database (2012)

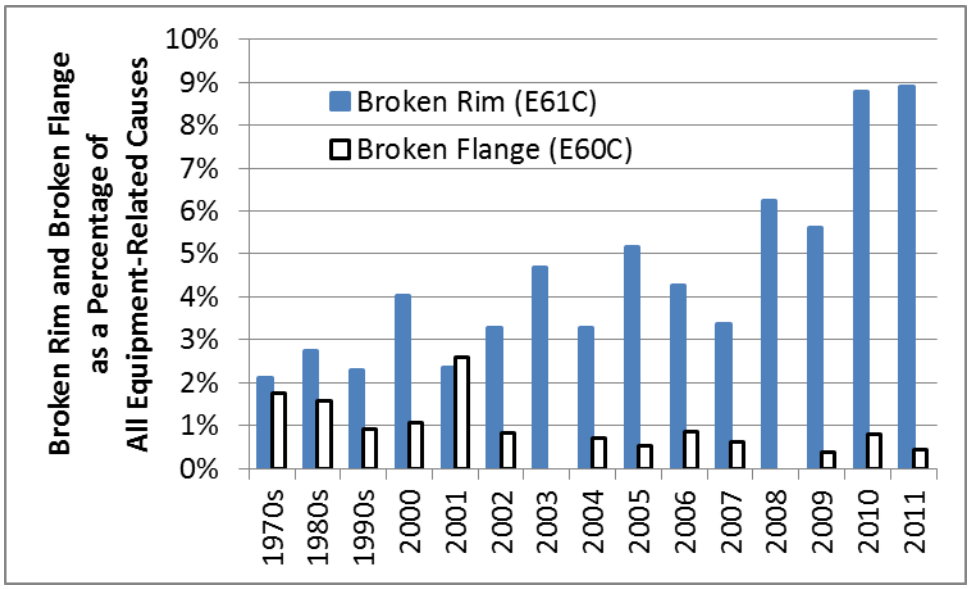

Figure 3. Broken Rim and Broken Flange Accidents as a Percentage of all Equipment-Related Accidents from FRA Safety Database

2.2 AAR Statistics and Rules

A wheel with a cracked or broken rim or a cracked or broken flange is condemnable according to the *Field Manual of AAR Interchange Rules*, Rule 41, 2012. The AAR has assigned Why Made Code (WMC) 68 for cracked or broken rims and WMC 66 for cracked or broken flanges. Shattered rim is covered in the same rule and is assigned WMC 71. The AAR car repair billing database shows that WMC 66, 68, and 71 are the cause for only a small percentage of wheel removals each year. Removals for these defects declined over the period between January 2001 and December 2009 in terms of percentage of wheels removed. Between January 2010 and December 2011, the WMC 66 and 68 removals increased as a percentage of all removals, while the WMC 71 removals decreased even further (AAR 2012). Figure 4 shows the removals as a percentage of all wheel removals in the AAR car repair billing database. Between January 2004 and December 2011, a total of 1,107 wheels were removed for WMC 66, and 2,075 wheels were removed for WMC 68. A total of only 596 wheels were removed for shattered rim during this same period. Annual average removals for these causes over the period January 2004 to December 2011 were 138, 259, and 75 for WMC 66, 68, and 71, respectively. This data, combined with the FRA safety statistics, shows that most wheels are identified and removed without a safety issue. Only 4 percent of wheels with broken rims or flanges result in a train accident ((137+14)/(1,107+2,075+596) * 100% = 4.00%).

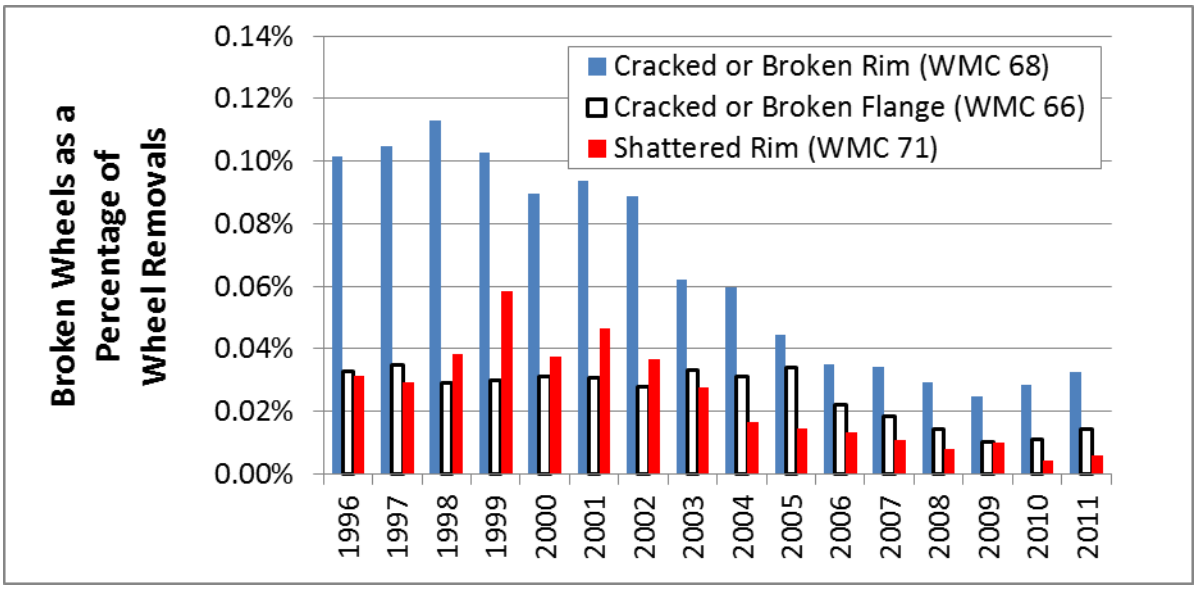

Figure 4. Wheel Removals for Cracked or Broken Rim, Cracked or Broken Flange, and Shattered Rim from AAR Car Repair Billing Database

In recent years, the AAR has established and/or tightened criteria that have a strong potential to improve wheel safety in the areas of UT, allowable dynamic wheel impact load levels, and microcleanliness testing. UT acceptance specifications for newly manufactured wheels were tightened in 1999 (Stahura 1999) and again in 2006 (Stahura 2006). Wheel shop UT specifications for reprofiled wheels were established in 2003 (Ameen 2002) and tightened in 2008 (AAR 2012, RP-631). All of the AAR UT criteria require the use of Distance Amplitude Correction, which effectively rejects defects of a specific size regardless of their depth in the rim. The reference defect for UT system calibration is a ⅛-inch-flat-bottom hole. Flaws are quantified as a percentage of the UT signal relative to the reference defect. Table 1 shows the AAR's current and historical UT specifications and the approximate diameter of the largest flaw that would meet the criteria.

Table 1. Current and Historical AAR UT Criteria

Effective Date Range	Applicability	Percent Signal for Rejection	Approximate Effective Diameter of Largest Allowable Defect
Before July 15, 1999	New Wheel	100	0.125 in
July 15, 1999, to June 1, 2006	New Wheel	50	0.088 in
June 1, 2006, to present	New Wheel	25	0.063 in
Before January 1, 2003	Reprofiled Wheel at Shop	N/A	No UT required
January 1, 2003, to June 30 ,2008	Reprofiled Wheel at Shop	50	0.088 in
July 1, 2008, to present	Reprofiled Wheel at Shop	25 (0.5- to 0.875-inch deep), 50 (deeper than 0.875 in)	0.063 in (0.5- to 0.875-inch deep), 0.088 in (deeper than 0.875 in)

In July 2003, the AAR implemented a rule to allow the removal of any wheel producing at least a 90,000-pound dynamic load as measured by a wayside wheel impact load detector. As of July 2005, wheels in cars that are on a shop track can be removed if they have produced at least an 80,000-pound impact load (Stahura 2005). A requirement for microcleanliness testing of new wheel samples was established in 2003 (Stahura 2003), and the requirements were tightened in 2008 (Stahura 2007). Six samples are prepared from a wheel, and the average and worst field area percent oxides, voids, and sulfides are evaluated. Table 2 lists the current and historical AAR microcleanliness limits.

Table 2. Current and Historical AAR Microcleanliness Criteria

Effective Date Range	Limit for Average Percent Area, Voids Plus Oxides	Limit of Worst Field Percent Area, Voids Plus Oxides	Limit of Worst Field Percent Area, Sulfides
November 1, 2003, to January 1, 2008	0.1%	1.0%	N/A
January 1, 2008, to present	0.1%	0.75%	0.75%

2.3 Previous Research

Broken wheels are an important topic of research as evidenced by the large body of available literature. Many shattered rim research papers were published in the 1990s and early 2000s. Focus started shifting from shattered rim research to VSR research in the mid-2000s.

2.3.1 Shattered Rim

The shattered rim wheel failure mode has been shown to be a classic fatigue problem with a subsurface crack that has defined periods of initiation, propagation, and failure. The wheel tread is left with clamshell beach marks parallel to the tread surface, indicating progressive crack growth (Berge 2000). This failure mode has been observed around the world in heavy haul freight service (Lunden 1992; Marais 1998) as well as high-speed service (Beretta, et al. 2001). The high strain rate associated with impact loading acts to reduce the endurance limit and is thought to be a major factor in the initiation of shattered rim defects in wheels (Stone, Lonsdale, and Kalay 2001). Calculations show that material flaws (voids or inclusions) of approximately 0.04 in (1 mm) can initiate shattered rim defects in the heavy haul freight service environment (Lunden 1992; Marais 1998); a 0.025-inch void was found at the origin of one shattered rim (Stone and Dahlman 2000). Larger material flaws decrease the necessity of an impact load for crack initiation (Stone, Lonsdale, and Kalay 2001). Shattered rims typically originate 0.5 to 0.75 in below the tread surface for heavy haul freight wheels (Stone and Dahlman 2000) and slightly shallower (0.4 to 0.6 in) for wheels in high-speed service (Beretta, et al. 2001).

Shattered rims can sometimes result in a combination shattered rim and VSR due to a final brittle fracture of the front rim face following consistent shattered rim fatigue crack growth in a deep horizontal plane (Stone, Tournay, and Cummings 2008). Such wheels should be considered shattered rims due to the root cause. Figure 5 shows a wheel with VSR crack that occurred long after the shattered rim defect had initiated and propagated.

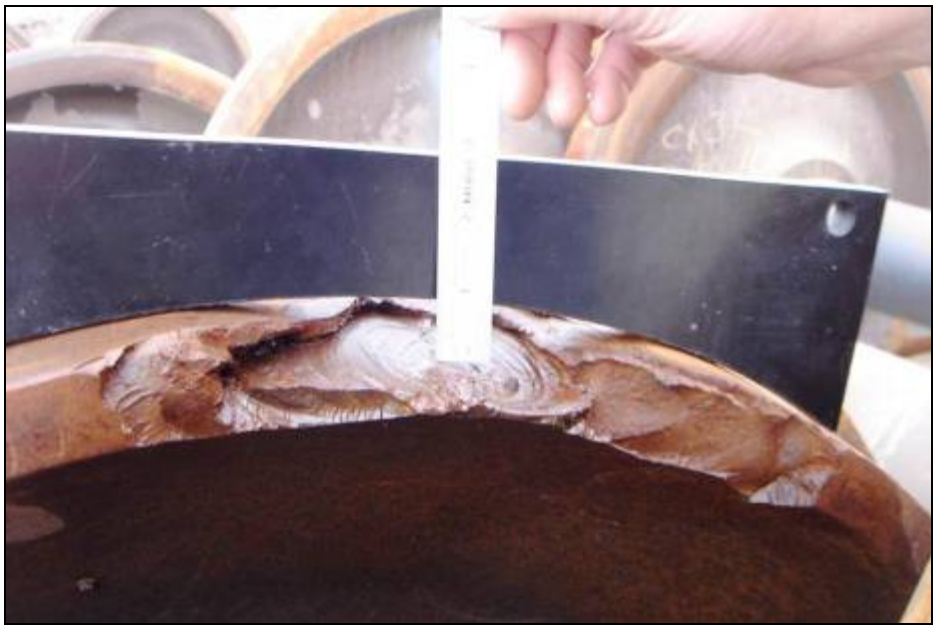

Figure 5. Shattered Rim Wheel with VSR in Combination

Microcleanliness test results of nine wheels with shattered rims showed that six would fail to meet the current AAR microcleanliness limit for average percent volume voids and oxides (Dahlman and Lonsdale 2003). Four of these wheels showed values more than four times the current AAR limit. Interestingly, the single VSR wheel reported in this same study met current AAR microcleanliness limits for average percent volume voids and oxides.

Literature sources disagree about whether shattered rims occur more frequently in new wheels or reprofiled wheels. The AAR wheel failure data shows that most shattered rims occur in wheels with more than 90 percent of the rim thickness remaining (Stone and Dahlman 2000). However, one North American wheel manufacturer reports that all of the wheels it analyzed with shattered rims had been reprofiled with an average tread loss of eleven-sixteenths of an inch (Berge 2000). All shattered rims in high-speed service wheels reportedly occurred in reprofiled wheels (Beretta, et al 2001).

Attempts to create shattered rims in the laboratory have proven successful using worn wheels that had been reprofiled during their service lives and then exposed to rolling contact loads from a dynamometer (Berge 2000). In one case, a service-worn wheel with a thin rim was subjected to standard wheel-rail normal forces of 36,000 lb for the equivalent of 40,000 miles (mi) on the dynamometer. UT did not show any subsurface cracks. The load was increased to 110,000 lb for the equivalent of 6,000 mi and a subsurface crack was detected with UT. After another 6,700 equivalent mi at 36,000 lb, the crack propagated to the front plate face. Similar attempts to create shattered rims in new wheels were unsuccessful.

Parametric finite element modeling and fracture mechanics were used to investigate the effect of wheel rim thickness, wheel load, residual stresses in the rim, and the size and location of material defects in the rim on shattered rim cracking (Sura and Mahadevan 2010). Variables studied and modeled were:

- Initial crack size
- Initial crack depth
- As-manufactured and service induced residual stress in the rim
- Vertical load on wheel tread
- Rim thickness

The prediction of crack growth for this report is based on the comparison of the stress intensity factor range created under load with the threshold stress intensity factor range. The vertical wheel load and initial crack depth appeared to have the most effect on the value of the stress intensity factor range. A crack depth of between 0.75 and 0.875 in was the most detrimental. Horizontal wheel load cases were not studied.

2.3.2 VSR

While the root causes of shattered rim have been identified and generally agreed upon by researchers around the world, the root cause of the VSR failure mode has been more elusive. Unlike shattered rim, VSR is not widely reported outside of North America. This begs the question: What is different about the North American railway system that creates the necessary conditions for VSR? A number of differences exist between the North American railway system and other heavy haul railway systems in the world, including the use of a higher percentage of cast wheels, different wheel maintenance practices, a colder winter environment, and a more demanding service environment in terms of grades and curves.

The manufacturing method of the wheels (cast or wrought) does not seem to have strong influence on VSR. The occurrence of VSR for cast and wrought wheels is representative of the relative populations based on AAR MD-115 wheel failure reports. However, maintenance practices and service environment could affect the quantity, size, depth, and time in service after formation of wheel shells and spalls. Shelling and spalling are indicated as potential precursors for VSR in a number of reports. The root causes of wheel shelling and spalling have been researched extensively and are beyond the scope of this report.

Two reports describe largely similar theories on the formation of VSR cracks (Dick, et al. 2008; Lonsdale and Oliver 2011). Tread damage on the wheel surface in the form of a shell or spall initiates cracking that propagates into a region of tensile residual stress in the rim. The tensile residual stress encourages further crack growth until a portion of the rim breaks free from the wheel.

Residual stresses have been regarded as an important factor in VSR formation since at least 2006 (Wang 2006). Parametric finite element modeling was used by a wheel manufacturer to investigate the effects of different parameters during heat treating of the resulting wheel residual stress. The analysis showed that the residual stress was especially sensitive to the creep properties used in the model and predicted a range of about 4 kilopounds per square inch (ksi) up to about 21 ksi for the axial residual stresses (Wang 2006). Modeling with an improved creep function shows that the heat-treating process leaves an area of residual tensile stress in the axial direction on the rim, with a maximum tensile value of more than 28 ksi (Pilch 2008). Such stress could act to promote crack propagation.

The wheel-rail contact patch of hollow worn wheels tends to be located closer to the front rim face compared with wheels with nonhollow profiles. The additional bending stress generated when the contact patch is located near the front rim face has been suggested as an influencing factor on VSR formation (Berge 2001). A comparison of the contact conditions of 66 VSR wheelsets and 108 service-worn wheelsets that had not failed due to VSR showed that the VSR wheelsets were more likely to contact the rail out near the front rim face of the wheel (Kristan, Stone, and Elkins 2004).

One attempt to create a VSR under controlled conditions is described in the literature. A drop hammer machine was used to deliver loads in excess of 200,000 lb to a service-worn wheel that had developed shelling on the tread (Lonsdale, Rusin, and Hay 2009). The test was not able to produce a VSR failure in the wheel and was halted after 30,000 impact events (Lonsdale and Oliver 2011).

An inspection of 71 VSR wheelsets was conducted and showed the following (Dick, et al. 2008):

- VSR typically occurs between 1 and 2.75 in from the front rim face.
- VSR failures progress in "jumps"—not classical fatigue and not a single fracture.
- The origin of the VSR is typically near a tread defect such as a shell or spall, but not always.
- VSRs can be found in wheels with a wide variety of diameters, designs, wear (rim thickness, flange thickness, and tread hollow), manufacturing methods, and can occur under many different car types and car gross tonnage ratings.
- Ten years was the most common service life for VSR wheels (manufacture date to failure date).
- Most VSR wheels have elevated levels of impact load prior to failure. However, more than half were below condemning limits and about 15 percent showed no notable impact loads.

Measurements of the axial residual stresses in new and service-worn wheels have been the recent focus of one wheel manufacturer (Lonsdale and Oliver 2011). Initial residual stress measurements were made with a core drilling technique on a new wheel and a VSR wheel. This data was reported as shallow as 0.010-inch radial depth below the tread surface. The new wheel showed residual compressive stresses in the circumferential and axial directions greater than 50 ksi to a radial depth of approximately 0.020 in and greater than 25 ksi to a radial depth of approximately 0.050 in. Measurements were reported to a depth of 0.300 in and remained compressive for the new wheel. For the VSR wheel, residual stresses in the circumferential and axial directions reached their compressive peaks at approximately 0.125-inch radial depth and transitioned from compression to tension at a radial depth of approximately 0.180 in. Axial residual stress in this VSR wheel reached a maximum tensile value of approximately 35 ksi at a radial depth of approximately 0.265 in. Additional residual stress measurements were made with an x-ray diffraction technique at coarser radial depth increments. This process allows residual stress measurements to be made at deeper radial locations. Data plots show that axial residual stresses were much larger in all service-worn wheels compared with new wheels. Tests were conducted on cast, wrought, heat treated (AAR Class C), and nonheat treated (AAR Class U) wheels at locations 1.5- and 3-inches laterally from the front rim face of the wheel. The measurements from a total of 19 wheels are reported. For the worn wheels (VSR and non-VSR), the axial residual stresses transition from compression to tension at radial depths 0.25 to 0.6 in

below the tread surface. Maximum tensile values between 10 and 25 ksi are shown. Maximum compressive values for the worn wheels are all at the shallowest depth measurement (approximately 0.2 in) and are in the range between 20 and 45 ksi. At 3 in from the front rim face, the axial residual stresses in VSR wheels reach much higher tensile values compared with other service worn Class C wheels (23 ksi compared to 10 ksi). Service worn Class U wheels reach their peak axial residual tensile values at radial depths much deeper than Class C wheels (1.1 in compared to 0.75 in). The authors suggest that this fact may contribute to more VSR cracks in Class C wheels because a crack would not need to propagate as far in the radial direction to reach an area of large tensile residual stress.

Additional residual stress testing was then conducted to explore the effects of impact loads on the residual stresses developed in the wheel rim (Lonsdale and Oliver 2012). Slices from seven wheels with total indicator runout (TIR) between 0.075 and 0.2 in were extracted for testing. TIR is used to quantify radius deviations around the wheel circumference and is a source of impact loads for wheels in revenue service. Two test samples were removed from each wheel: one from an area with large TIR values where impact loads were expected and one from an area with low TIR values where no impact loads were expected. The samples from the low TIR areas of the wheels produced fairly consistent values of axial residual stress as a function of radial depth. The samples from the high TIR areas were less consistent and produced higher compressive axial residual stress near the tread surface compared with the samples from areas of low TIR. Average tensile axial residual stress was similar between the sample groups.

One wheel manufacturer retrieved the UT data recorded immediately after the manufacture of 26 wheels that later developed VSR cracks in service (Lonsdale and Oliver 2012). The manufacturer reports that the distribution of UT signals was similar to a large sample of normal production wheels. Further, they report that the sulfur and phosphorus content of the 26 VSR wheels was less than the average content of these elements in normal production wheels. These are indications that wheels that are free of relatively large manufacturing defects (voids and inclusions) and have good microcleanliness can still develop VSR cracks in service.

Finite element analysis and fracture mechanics were used to study the VSR failure mode in a project jointly funded by TTCI, Griffin Wheel, and Standard Steel (Sura and Mahadevan 2010). Findings of the parametric modeling were as follows:

- Proximity of the wheel-rail load to the crack is extremely important in triggering VSR failures. The closer the load to the crack, the higher the probability of VSR.
- Cracks parallel to the front rim face are critical.
- Load magnitude is an important factor; higher loads give a higher probability of VSR.
- The critical depth for VSR cracking depends on the load location and crack orientation. Cracks at depths up to a quarter of an inch and oriented parallel to the front rim face are critical for VSR cracking.
- The probability of VSR increases proportionally to the square root of the crack size.
- Rim thickness and residual stress state* are not dominant parameters in triggering VSR.

- High axial stresses develop in the middle of the rim because of the manufacturing process and mechanical loading on the tread surface. However, it is not clear how or if this contributes to VSR failure.

*Note that recent axial residual stress testing has shown axial tensile residual stresses much larger than those applied in the parametric simulations. This may invalidate the simulation conclusions regarding the effects of residual stresses.

2.4 Section Summary

The number of broken rim accidents has increased slightly in recent years and are increasing as a percentage of all equipment-related accidents. Shattered rims are on the decline, likely due to a combination of AAR rule changes for wheels regarding tighter UT limits on allowable defects, tighter microcleanliness limits, and the establishment of a maximum impact load criteria. Shattered rims have been created successfully under controlled laboratory conditions. VSRs are thought to be the result of tread damage on the wheel surface in the form of a shell or spall that initiates cracking in the rim and produces impact loads when it contacts the rail (Dick, et al. 2008; Lonsdale and Oliver 2011). If the crack propagates vertically to an area of tensile residual stress in the wheel rim, further crack growth is encouraged until a portion of the rim breaks free from the wheel. VSRs are not reported outside of North America and the only reported attempt to create a VSR under controlled conditions was not successful.

3. Inspection

Visual and ultrasonic inspections were conducted on wheels that developed VSR cracks and their mate wheels on the other end of the axle. Data on these wheels, including the impact loads the wheels produced in service, was analyzed.

3.1 Visual Inspection

TTCI requested and received a total of 29 VSR wheels and 6 broken flange wheels from 3 different railroads to analyze the fracture surfaces and conduct laboratory tests. Basic data was collected from the wheels regarding manufacturer, manufacture date, bearing locking plate date, car number from which the wheelset was removed, removal date, and rim thickness. Next, wheel profiles were recorded for each wheel and analyzed for flange height, flange thickness, and tread hollow. After TTCI completed the initial inspection, a group of wheel experts was convened to visually inspect each wheel tread surface for evidence of shelling and spalling and determine the failure origin location based on any low-cycle fatigue "beach marks" that developed during failure. Appendix A contains details of each inspected wheel.

Thirty-one of the broken wheels inspected by TTCI were cast, and four were forged. All of the wheels were AAR Class C (heat-treated). The wheelsets were removed from a variety of car types including 11 covered hoppers, 9 coal hoppers or gondolas, 5 boxcars, 4 stack cars, 3 flat cars, and 2 tank cars. The gross tonnage rating of the single unit cars was as follows: 16 cars at 110 tons, 14 cars at 100 tons, and 1 car at 70 tons. Single-wear wheel designs outnumbered double-wear designs by 24 to 11. Any wheelset for which the bearing locking plate date was more than a few months newer than the wheel manufacturing date was assumed to have been reprofiled at least once. Using this methodology, TTCI determined that 18 of the broken wheels had been reprofiled while 12 were in their initial life cycle. Bearing locking plate dates were not available for the remainder of the wheelsets. Median time from manufacture to failure was 5.4 years with a maximum of 18 years and a minimum of 8 months. Median time from bearing locking plate date to failure was 2.3 years with a maximum of 10.6 years and a minimum of 8 months.

Rim thickness of the VSR wheels ranged from 0.88 to 1.94 in with a median rim thickness of 1.31 in. Rim thickness of the broken flange wheels ranged from 1 to 1.19 in with a median rim thickness of 1.13 in.

One VSR wheel was found to have a severe 6 mm hollow tread as the apparent result of sustained contact between the tread surface and the brake head. Six of the other broken wheels inspected had hollow treads ranging from 0.5 to 3 mm. The balance of the broken wheels had no hollow wear. With the exception of the VSR wheel with brake head wear, each mate wheel typically had a magnitude of hollowing similar to the broken wheel on the same axle. Flange thickness of the broken wheels ranged from 1.01 to 1.38 in with a median of 1.25 in. The VSR wheel with the brake head wear had a flange that was 0.33 in thinner than its mate. For all of the other wheelsets inspected, the broken wheel and mate wheel had similar flange thicknesses typically within 0.1 in. Flange height of the broken wheels ranged from 1.01 to 1.48 in with a median of 1.18 in. Flange height differences between the broken wheel and its mate were

typically less than 0.05 in and never more than 0.15 in. Flange thickness, flange height, and tread hollow were similar between the broken flange wheels and the VSR wheels.

The location of the origin of the failure was determined by visually examining the failure surface. VSR and broken flange wheels usually exhibit faint markings on the failure surface that show the direction in which the crack propagated. By tracing these marks backwards, an origin point was established for each broken wheel. The radial depth of the origin point was then established relative to the existing tread surface and the axial location was established relative to either the front rim face or the back of the flange. Origin radial depths were similar for both VSR and broken flange wheels and ranged from 0.10 to 0.25 in below the tread surface with a median value of 0.17 in. Figure 6 shows a histogram of the origin radial depth relative to the worn tread surface. For VSR wheels, axial locations of the origin ranged from 1.25 to 2.60 in from the front rim face with a median value of 2.10 in. For broken flange wheels, axial locations of the origin ranged from 3 to 3.75 in from the front rim face with a median value of 3.25 in.

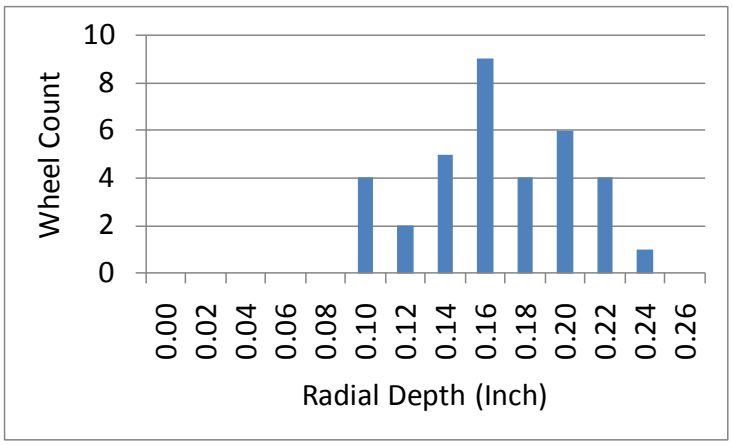

Figure 6. Histogram of VSR Origin Depths Relative to Worn Tread Surface

Figure 7 shows the axial and radial locations of the failure origins. The radial dimensions of this figure have been referenced to the tapeline of a brand new wheel by incorporating the origin radial depth below the worn tread surface and the tread wear as determined by the difference in rim thickness from the nominal rim thickness. Although the origins are at a consistent radial depth from the worn tread surface, the radial depth varies considerably when referencing the new wheel tread surface. This is an indication that broken wheels are not typically the result of microstructures such as bainite or martensite formed near the tread surface from the quenching operation during the manufacturer's heat treatment.

TTCI noted shells on the tread surface in close proximity to the origin point for 23 of 29 VSR wheels and all 6 broken flange wheels. Usually, when tread damage is the result of a wheel-sliding event, martensite is present on the tread surface. Etching the tread surface near the shells of the broken wheels did not reveal any martensite, implying that the shells were not the result of a wheel-sliding event. Rolling contact fatigue and thermal mechanical shelling are the likely causes.

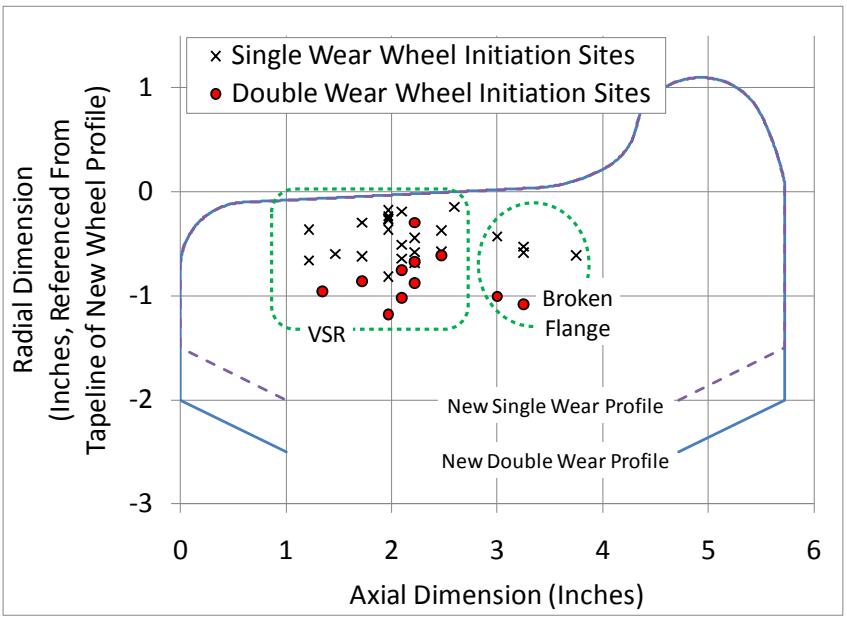

Figure 7. Origin Locations Relative to New Wheel Profiles

3.2 Impact Loads

The wheel impact load detector (WILD) data history from each broken wheel was analyzed. Figure 8 contains a histogram of the highest impact load for each broken wheel up to and including the official failure date. For some wheels, the failure may have occurred prior to passing a WILD site, and therefore the impact load would indicate the conditions after the failure rather than the conditions immediately prior to failure. Sixteen of the broken wheels analyzed had exceeded the AAR limit of a 90,000-pound impact load prior to removal.

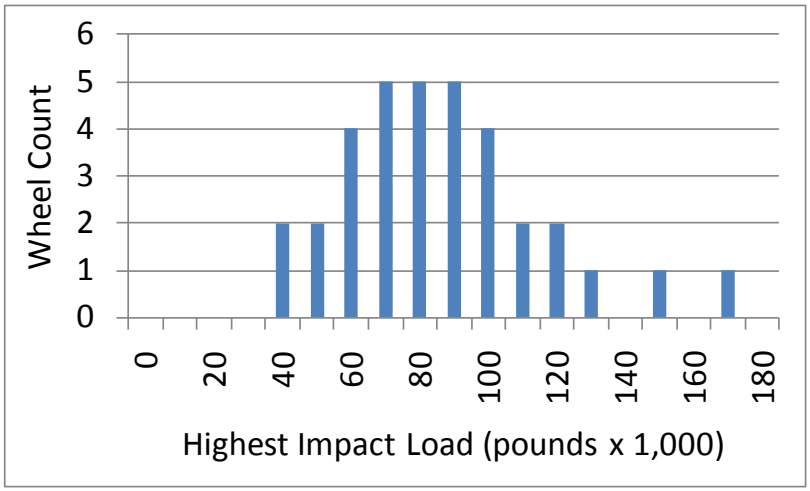

Figure 8. Histogram of WILD Data

Another way to analyze WILD data is by calculating "kip days." A kip is a unit of force equal to 1,000 pounds. The kip-day calculation is a way to identify wheels that have been producing noncondemnable impact loads for a long time. A wheel begins accumulating kip days the first time it exceeds a 30,000-pound dynamic load limit (impact load minus average load). Each day thereafter, the highest impact load (in kips) experienced by that wheel is added to the kip days total for the wheel. For example, a wheel with a maximum impact load of 70 kips (70,000 lb) would have a daily accumulation of 70-kip days. The kip days total for a wheel is rezeroed when the wheelset is changed. One railroad has suggested that 11,000-kip days could be used as a limit. Figure 9 shows that if an 11,000-kip day removal criterion was used along with the current 90,000-pound impact load limit, 24 of the 35 broken wheels would have been condemnable based on WILD readings.

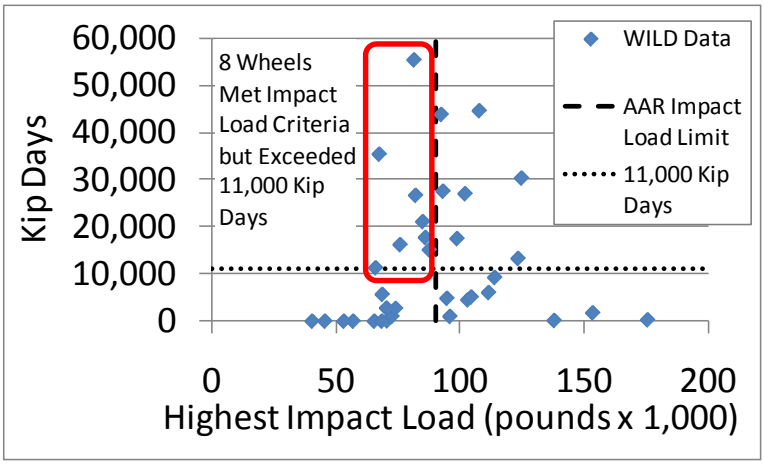

Figure 9. Kip Days and Highest Impact Loads

3.3 Ultrasonic Inspection

Cracks in wheels can be found using UT equipment. Each broken wheel and its mate were scanned for horizontal UT indications in the axial-circumferential plane (with the probe on the tread surface aimed radially toward the hub) and for vertical UT indications in the radial circumferential plane (with the probe on the front rim face aimed toward the back of the flange). Dual element probes of 2.25 MHz and 5 MHz were used to detect horizontal indications. A 2.25 MHz standard zero probe was used to detect vertical indications.

TTCI found 111 horizontal UT indications on 27 of the 35 broken wheels. No horizontal UT indications were found on the other eight broken wheels. The UT indications are considered subsurface cracks rather than manufacturing defects such as voids or inclusions because of their large size. The horizontal UT indications ranged in size from 0.1 in^2 to 24.7 in^2 with a median value of 1.3 in^2. The radial depth of the horizontal UT indications ranged from 0.11 in to 0.60 in with a median value of 0.21 in. Figure 10 shows the depth and area of the horizontal UT indications found in the broken wheels. The majority of the horizontal UT indications (83 percent) were found in the same range of radial depths as the expected maximum stress and the failure origins.

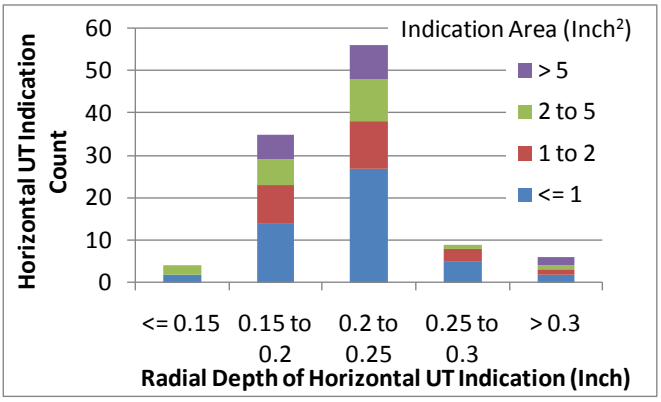

Figure 10. Size and Depth of Horizontal UT Indications

Horizontal UT indications were found in the immediate vicinity of the failure origin on 13 of the broken wheels. Figure 11 shows an example of a broken wheel with a large horizontal UT indication (outlined in white paint) marked around the VSR origin.

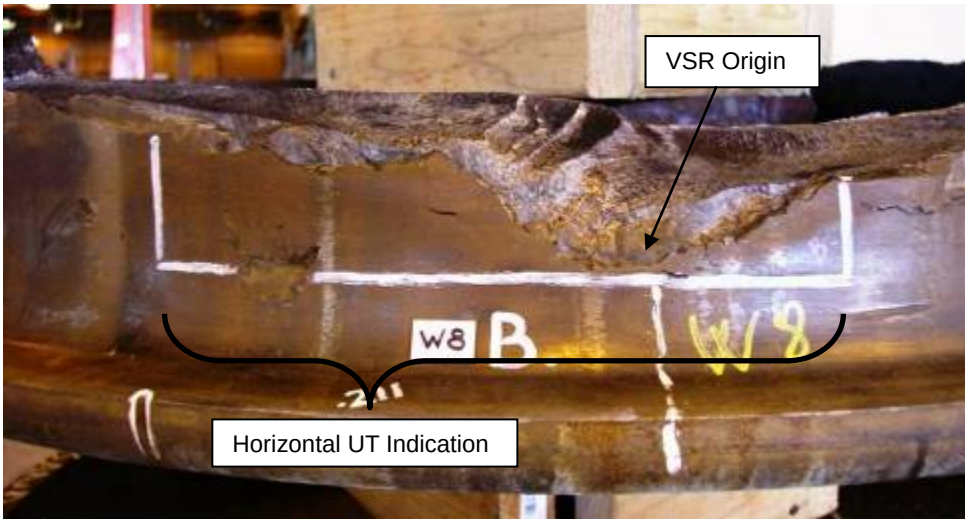

Figure 11. VSR Wheel with a Large Horizontal UT Indication Surrounding VSR Origin

TTCI found 52 horizontal UT indications on 18 of the 35 mate wheels. No horizontal UT indications were found on the other 17 mate wheels. The horizontal UT indications ranged in size from 0.1 to 28.8 in^2 with a median value of 1.1 in^2. The distribution of indication depths and sizes was similar for both the broken wheels and the mate wheels.

Vertical UT scanning was conducted on the broken wheels and their mates to identify any vertically oriented indications and to determine if the VSR or broken flange crack extended beyond the portion that was visible. Based on vertical UT indications, the failure crack extended around the circumference of the wheel beyond the portion that was visible for 16 of 35 VSR and broken flange wheels. Extension of the cracks ranged from 1 to 25 in around the circumference

with a median value of 3.4 in. No other vertical UT indications were found on the broken wheels or their mates.

3.4 Subsurface Cracking

A common feature found on many of the broken wheels was a horizontal (approximately parallel to the tread surface) separation between two visually distinct layers in the wheel rim. Figure 12 shows examples of two VSR wheels with distinct upper and lower layers in the rim. The upper layer is typically no more than 0.25 in thick and the lower layer is comprised of the remainder of the rim thickness. The upper and lower layers frequently have different axial widths. In some wheels, the upper layer extends axially past (overhangs) the VSR crack in the lower layer. In other broken wheels the opposite is found: the horizontal surface of the lower layer is exposed because the upper layer has shelled out or broken off above it. For both wheels pictured in Figure 12, the upper layer overhangs the VSR crack in some circumferential locations and has broken off the lower layer at other locations.

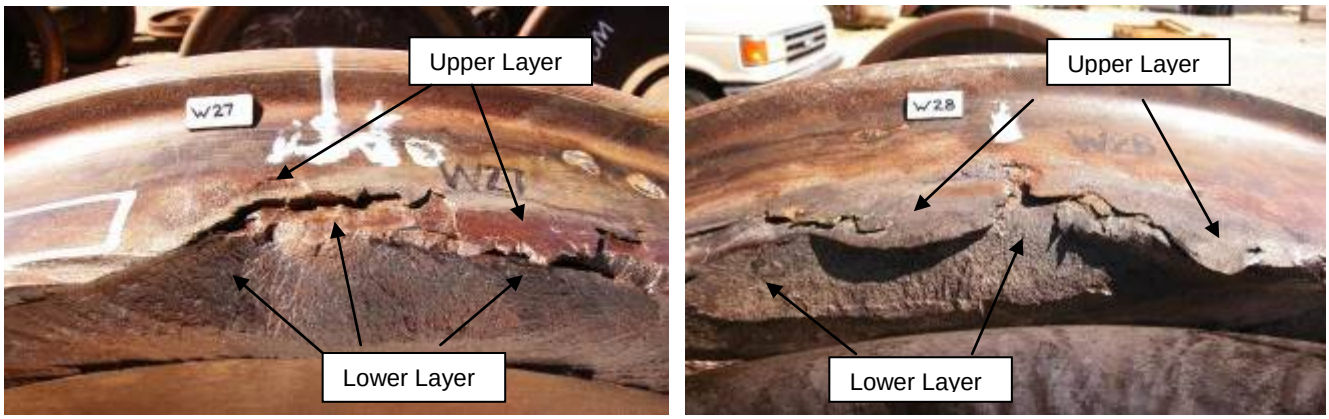

Figure 12. Examples of VSR Wheels with Two Distinct Horizontal Layers in the Rim

Figure 13 shows a wheel section with a horizontal crack that ranges in radial depth from about 0.1 to 0.25 in below the tread surface and a vertical crack that intersects the horizontal crack at a 0.18-inch radial depth. These dimensions are typical of most of the horizontal UT indications on the broken wheels and the radial depths of the VSR origins (where the horizontal crack turned into a vertical crack). The horizontal crack in this wheel separates the upper and lower layers of the rim.

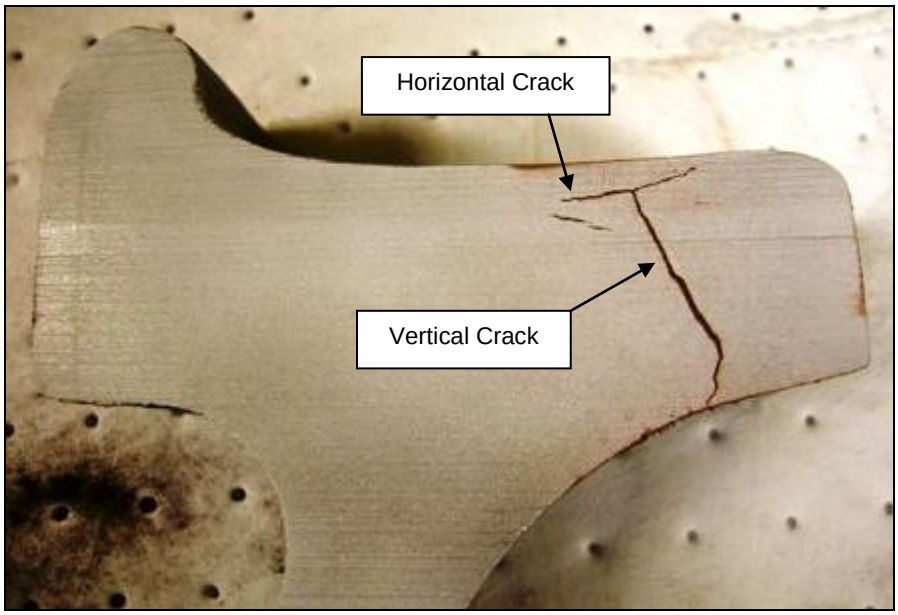

Figure 13. Branching between a Horizontal Subsurface Crack and a Vertical Crack

The horizontal separation of tread layers associated with VSR and broken flange wheels has been shown previously. However, it has typically been attributed to shelling rather than subsurface cracking (Berge 2001). Sketches of the transverse profiles of four broken wheels show a shallow horizontal component to the vertically broken piece. Figure 14 shows these profiles.

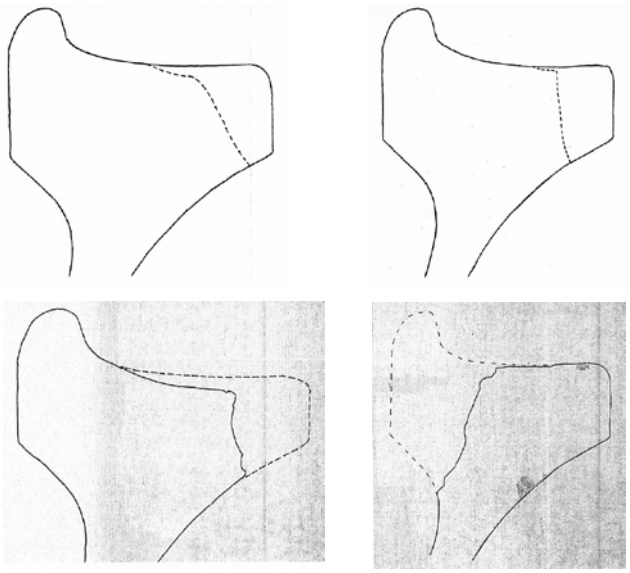

Figure 14. Sketches of VSR and Broken Flange Wheel Profiles Showing the Broken Piece with a Dashed Line (Berge 2001)

3.5 Destructive Evaluation

The majority of VSR wheels are discovered after the crack has caused complete separation between a piece of the rim and the remainder of the wheel. The broken piece is occasionally recovered for evaluation, but the typical VSR wheel failure is examined by looking at the cracked surface of the broken wheel without the benefit of the missing portion of the rim. Several representative VSR crack surfaces were extracted and examined under an optical microscope, but in each case, the two faces of the cracked rim had rubbed and grinded on each other while the wheel was rolling and before separation had occurred. This makes it difficult to accurately evaluate the crack origin for any type of material weakness such as a void or nonmetallic inclusion.

One of the VSR wheels provided for the inspection (assigned identification of "W43") was removed from service prior to the crack causing complete separation of the rim. A portion of the crack had propagated to the rim fillet allowing for discovery by visual inspection. Although the crack faces had rubbed against each other while the wheel was in service, the damage from this rubbing was somewhat less than a typical VSR wheel that has propagated to rim separation. Figure 15 shows the tread surface and plate of the wheel. White paint lines on the tread identify the approximate outline of a subsurface horizontal crack found using UT equipment. Figure 16 shows one side of the cracked rim after it had been extracted from the wheel and the crack had been opened to expose both surfaces. Two potential crack origins were identified as indicated with arrows marked A and B in Figure 16.

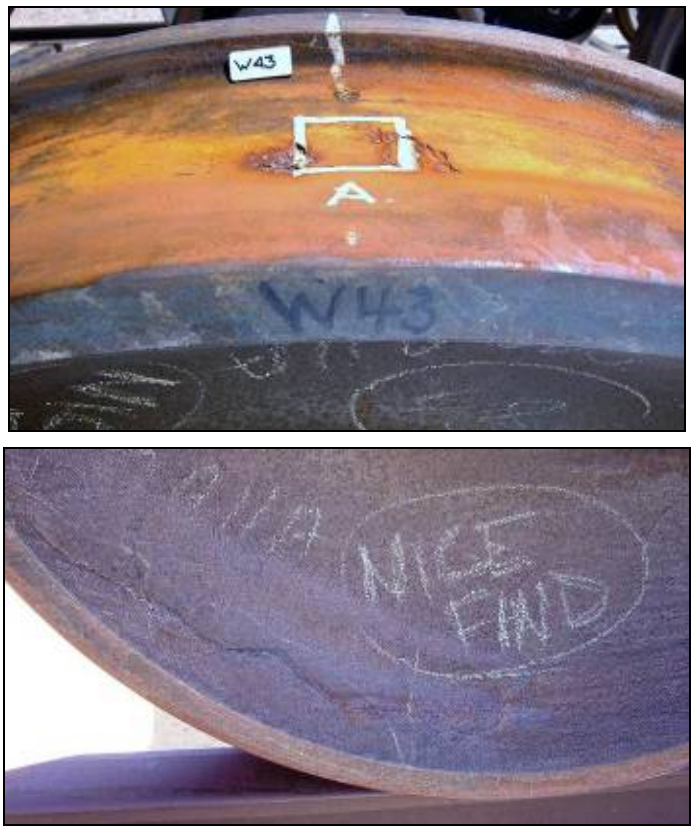

Figure 15. VSR Wheel W43 Tread (Top) and Plate (Bottom) Prior to Opening Crack

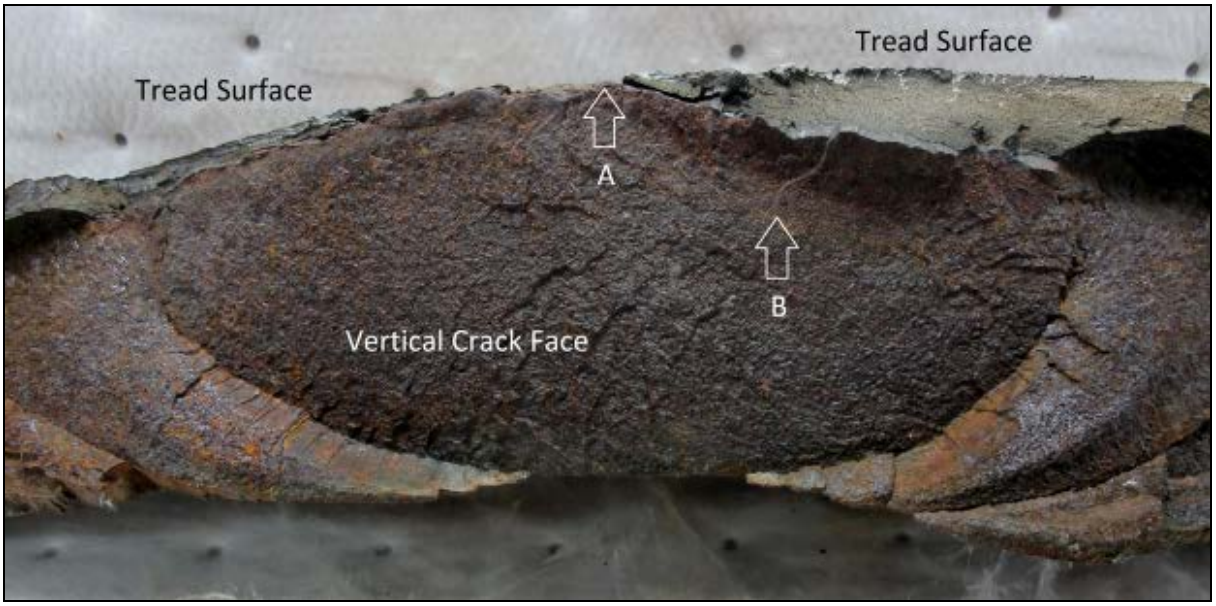

Figure 16. Potential Crack Original Locations on W43 after Opening Crack

Understanding the propagation path of a crack can help define the relative influence of high stress levels and localized material weaknesses. Nonmetallic inclusions act as stress concentrators and tend to solidify at the grain boundaries as ingots solidify and cool. The vertical crack faces from W43 were investigated using Norfolk Southern's scanning electron microscope (SEM). Samples from each side of the crack near the two potential initiation sites were extracted perpendicular to the crack plane, polished, and etched with a saturated solution of picric acid to show the microstructure, including the boundaries between prior-austenite grains. These samples were then viewed using the SEM. The crack appeared to propagate through the middle of grains (transgranular) rather than between prior-austenite grain boundaries (intergranular) indicating that high stress levels rather than material weakness were likely the main driving force in the crack propagation. However, during SEM analysis, it was difficult to identify the exact location of the potential vertical crack initiation sites. Once the crack had grown to a sufficient size, it was expected that the stress concentration created by the crack would increase the probability of transgranular propagation. Separating the rim material at the crack was necessary to examine the morphology of the crack surfaces and identify potential crack initiation sites. However, this required that the mating crack surfaces be viewed separately under the SEM, which made it difficult to confidently match crack asperities between the surfaces. This further reduced confidence in the finding that the crack experienced transgranular propagation. The ideal specimen for this type of analysis would be extracted from a wheel rim at the initiation site of a VSR crack at the initial stage of growth. Unfortunately, identifying such a wheel and extracting a sample at the VSR crack origin location is improbable. Figure 17 shows an example of some transgranular crack branches on one side of the W43 VSR crack surface.

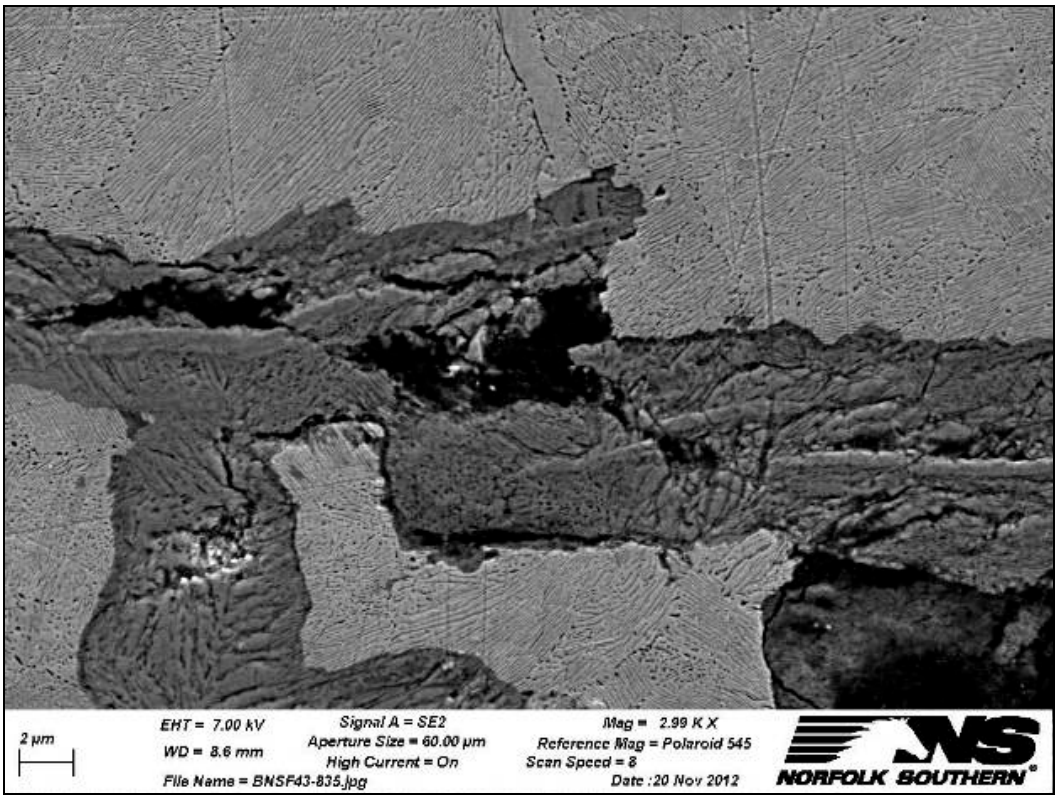

Figure 17. Transgranular Crack Branching (image courtesy of Norfolk Southern)

3.6 Section Summary

Inspections of 29 VSR wheels and 6 broken flange wheels showed a broad range of wheels including cast and forged wheels, reprofiled wheels and wheels in their first life cycle, and wheels removed from many different car types, including cars with gross rail load ratings of 110, 100, and 70 tons. Only a few of the VSR wheels had hollow worn profiles and the flange height, flange thickness, and rim thickness values were considered in the normal expected range. A VSR origin location was identified for each wheel and radial depths of these origins were all found in a tight band ranging from 0.10 to 0.25 in below the tread surface with a median value of 0.17 in. Shells were noted on the tread surface in close proximity to the origin point for 29 of the 35 wheels. If an 11,000-kip day removal criterion was used along with the current 90,000-pound impact load limit, 24 of the 35 broken wheels would have been condemnable at the time of their removal based on WILD readings. UT revealed horizontal cracks in 27 of the 35 broken wheels with a median value of 1.3 in^2 and horizontal cracks in 18 of the 35 mate wheels with a median value of 1.1 in^2. A common feature found on many of the broken wheels was a horizontal separation between two visually distinct layers in the wheel rim typically occurring no more than 0.25 in below the tread surface. Analysis of crack initiation site of VSR wheels is difficult because of the rubbing of the two faces of the crack surface prior to the final separation of the rim. The crack in one VSR wheel appeared to propagate through the middle of grains (transgranular) rather than between prior austenite grain boundaries (intergranular) indicating that high stress levels rather than material weakness were likely the main driving force in the crack propagation.

4. Test

Laboratory testing was conducted on the inspected VSR and broken flange wheels to explore some of the properties—microcleanliness and residual stress, for example—of the wheels.

4.1 Fatigue Crack Growth Rate

Fatigue crack growth rate testing was conducted on six samples extracted from two AAR Class C wheels to define the lower boundary of the value of the stress intensity factor that will cause a fatigue crack to grow. Tests were conducted at room temperature according to ASTM E647-08. Two specimens each were tested at stress ratios of 0.05, 0.2, and 0.5. This data is important for establishing the predicted crack growth due to an individual load cycle in which the stress intensity factor generated at the crack tip is known or estimated. Although these results were not applied directly to any work in this research project, they will enable finite element models to more accurately predict fatigue failures (such as shattered rim) in the future. Table 3 shows the stress intensity threshold results of the test. Appendix B shows a plot of the crack growth rates of each specimen as a function of the stress intensity factor.

Table 3. Stress Intensity Thresholds

Stress Ratio (R)	Wheel 1 Stress Intensity Threshold (ksi*√inch)	Wheel 2 Stress Intensity Threshold (ksi*√inch)	Average Stress Intensity Threshold (ksi*√inch)
0.50	5.14	4.06	4.60
0.20	10.11	5.13	7.62
0.05	8.40	5.88	7.14

4.2 Microcleanliness

Standard AAR microcleanliness testing of a newly manufactured wheel requires the analysis of six metallographic samples taken at equal spacing around the circumference of the wheel (approximately every 60 degrees). The evaluation surface of each sample is ⅞-inch long in the circumferential direction, located ½ in below the tread surface, and 2½ to 3¼ in from the back rim face (M-107/M-208 2011).

Microcleanliness tests were conducted on 25 VSR wheels and 5 broken flange wheels. Because these wheels were service worn and fractured, slight changes to the standard AAR microcleanliness test sample locations were necessary. Six samples were harvested from each wheel: two samples from each of three circumferential locations, spaced about 60 degrees apart on the portion of the wheel that was not fractured. At each circumferential location, one sample was harvested from the flange area and one from the tread area, as Figure 18 shows.

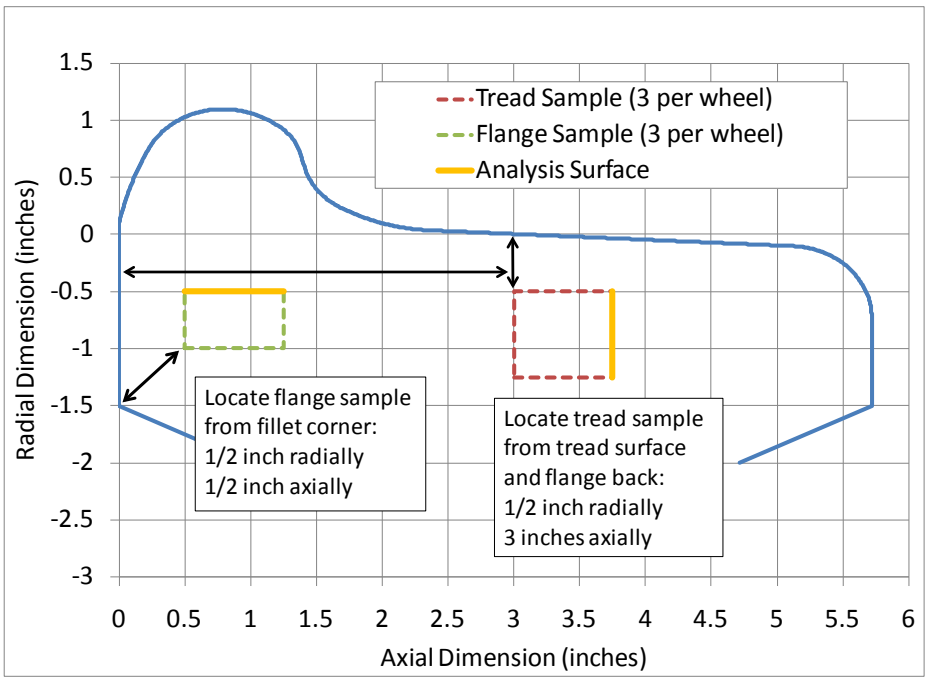

Figure 18. Microcleanliness Sample Locations

The analysis surface of the flange sample was perpendicular to the flange back (similar to the standard AAR analysis surface), while the analysis surface of the tread sample was parallel to the flange back and located at the axial dimension where VSRs most commonly initiate. The changes to the tread sample were made to try to better assess the microcleanliness in the area and orientation that would be most critical to VSR. Because the microcleanliness test can only evaluate a tiny fraction of a wheel, it is intended to be a general indicator of steel cleanliness. Thus, the flange samples should also provide relevant data about the steel cleanliness even though they are not harvested from the exact same location as the standard AAR test requirements. The AAR's Wheel, Axle, Bearing, and Lubrication Committee approved the sample locations prior to harvesting.

Sample preparation and analysis was conducted according to AAR specifications. Figures 19 and 20 show the microcleanliness results of the VSR and broken flange wheels compared with AAR limits in terms of average volume percent and maximum volume percent, respectively. All but two of the wheels met the current AAR microcleanliness limits and most wheels met the current limits by a wide margin. Both wheels that exceeded AAR limits failed because of VSR and were manufactured prior to the AAR microcleanliness requirement.

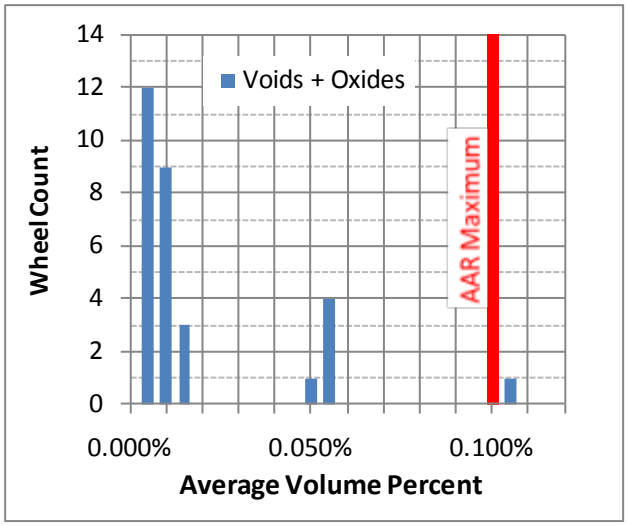

Figure 19. Histogram of Average Volume Percent Microcleanliness Results

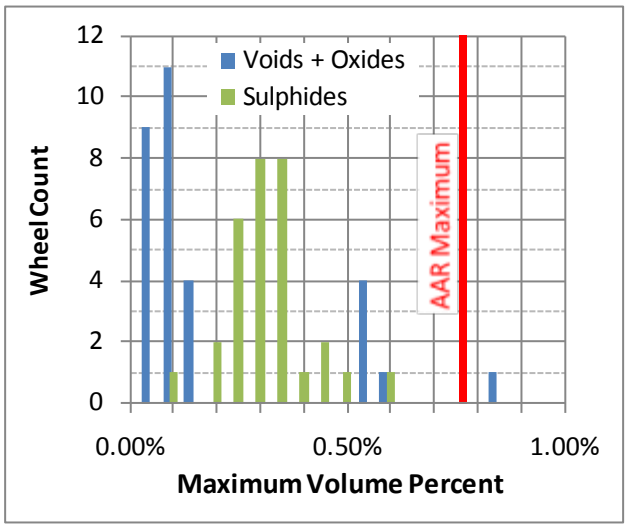

Figure 20. Histogram of Maximum Volume Percent Microcleanliness Results

These test results show that failure of the AAR microcleanliness test is not a prerequisite for VSR or broken flange failure. In a bulk sense, the steel in the wheels tested appears to be typical of many wheels in service today. Therefore, these results would not provide support for further tightening of the limits associated with the current AAR microcleanliness test. Unfortunately, the fracture surface of VSR and broken flange wheels nearly always sustains significant damage while in service making it nearly impossible to obtain conclusive evidence about voids or inclusions in the immediate fracture area that may have caused or contributed to the failure. Destructive microcleanliness tests only examine a tiny percentage of the steel in a tiny percentage of the wheels produced. As nondestructive testing methods improve, it may become practicable to substantially reduce the allowable defect size in both new wheels and reprofiled wheels.

4.3 Thermal History

Examining the microstructure and hardness of wheel steel can provide an estimate of the highest temperature the wheel experienced while in service. Fifteen of the wheel tread samples used for the microcleanliness test were repolished, etched with a saturated solution of picric acid, and photographed at a magnification of X1,000. Rockwell hardness testing was conducted at the center of each sample. Following manufacture, AAR Class C wheels normally have a pearlitic microstructure ½ in below the tread surface. All of the samples were extracted at least ½ in below the new tread surface.

By comparing the microstructures of each sample with other samples of wheel steel that had been exposed to controlled temperature conditions (Dedmon 2009), a range of maximum temperatures was estimated for each of the 15 samples. Figure 21 shows these estimates. The published data regarding the microstructure following controlled thermal exposure was gathered using samples of wheels that had not been exposed to the service environment and therefore did not have any work hardening in the wheel rim. Because of this difference, the 15 samples all had hardness readings higher than the comparison wheel samples from the literature and therefore hardness could not be used to help increase confidence in the estimated thermal history.

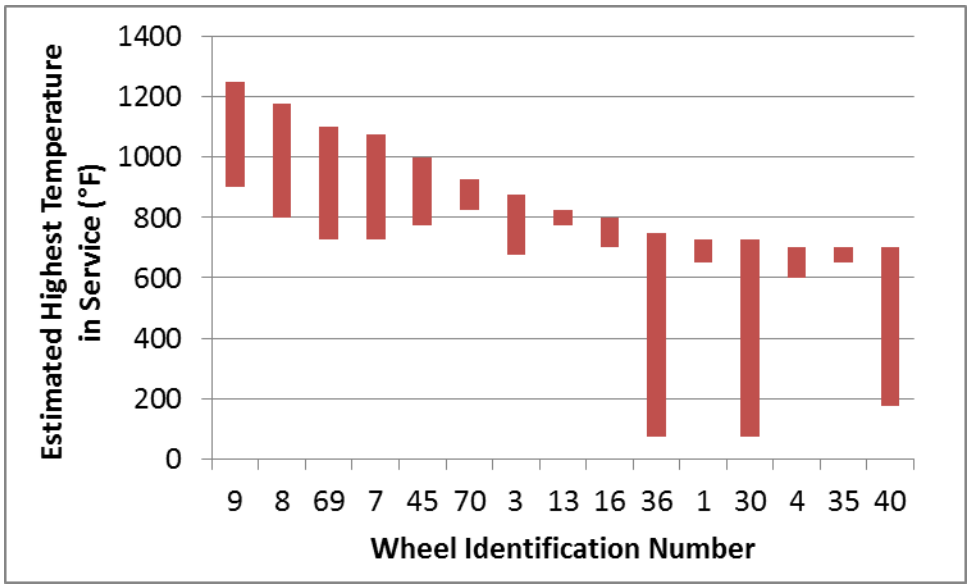

Figure 21. Estimated Maximum Temperature of Wheels

The maximum temperature estimates of the wheel samples show that 5 out of the 15 VSR wheels examined may have been exposed to temperatures of 1,000 °F or greater while in service, resulting in substantial spheroidization of the microstructure. This transformation results in a decrease in strength and fatigue life and could potentially play a role in wheel shelling and VSR formation.

4.4 Residual Hoop Stress

Tensile residual stresses can add to the mechanical stresses developed during wheel-rail contact and increase the probability for crack initiation and propagation. Compressive residual hoop

(circumferential) stresses are developed in the wheel rim both during manufacturing and from contact with the rail during service. Heat input from braking can relieve the residual hoop stress or, in some cases, cause an undesirable tensile state of residual hoop stress.

While harvesting the samples for the microcleanliness testing, data was collected during the first cut of each wheel to determine whether the wheel was in a state of tensile or compressive residual hoop stress (Rajkumar and Stone 1987; Galbraith, Ames, and Leister 2011). Following the method referenced above, each wheel was laid flat on a band saw table and cut along the radial plane at a circumferential location as far as possible from the fracture surface, as Figure 22 shows. A clip gage mounted on the wheel flange was used to determine the changes in the width of the kerf (cut opening) with respect to the radial depth of the cut. A widening kerf (positive slope when plotting cut opening versus cut depth) indicates that the blade tip is cutting through material in tensile residual hoop stress and a narrowing kerf (negative slope) indicates compressive residual hoop stress. Cutting fluid was constantly supplied during saw cutting to minimize thermal expansion effects.

Figure 23 shows plots of the changes in the kerf width as a function of the cut depth for each wheel. A new single wear wide flange wheel is also shown to provide a visual reference for the cut depth. For many of the wheels, the kerf increased in width during the initial 0.25 in of the cut depth indicating tensile residual hoop stress in the outermost tip of the flange. However, the kerf decreased in width for all wheels as the blade progressed further into the flange and rim indicating that all of the wheels were in a state of residual compressive hoop stress as desired. This state of stress would indicate that none of these wheels had been exposed to extreme heating immediately prior to VSR or broken flange failure. Any tensile residual hoop stress in the tip of the flange should not have a significant effect on VSR or broken flange failures that initiate near the tread surface.

Figure 22. Photo of a Saw Cut Test

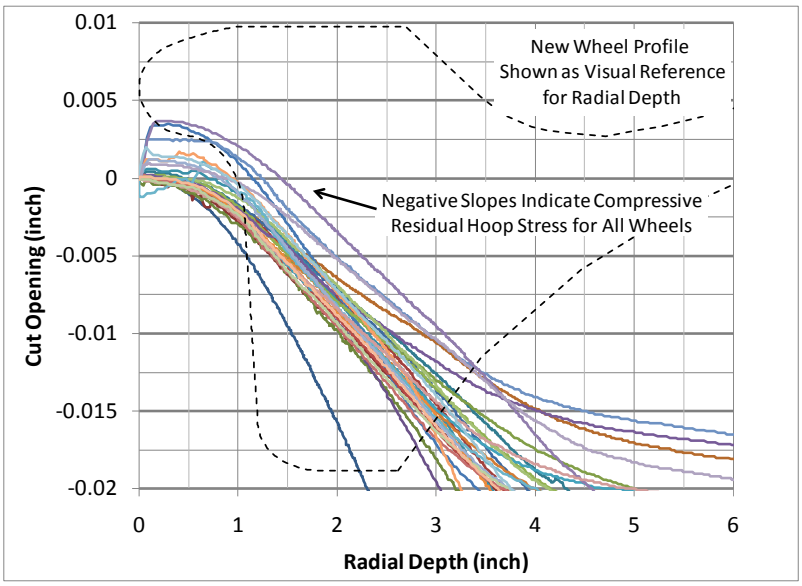

Figure 23. Saw Cut Results Showing Compressive Residual Hoop Stress for All Wheels Tested

The results from the thermal history tests and the residual hoop stress tests seem to contradict each other to some degree until examined further. The thermal history testing showed at least five wheels with estimated maximum temperatures that may have exceeded 1,000 °F, yet the residual hoop stress testing showed that all of the wheels were in a state of compressive residual hoop stress. Normal wheel-rail contact causes plastic deformation in the wheel rim, which imparts compressive residual hoop stress in the wheel. It is plausible that some wheels are temporarily heated in service to temperatures sufficient to cause changes in the microstructure (and change the residual stress state from compressive to tensile), but return to a state of compressive residual hoop stress after they cool down and experience normal cold working. This implies that none of the wheels failed while they were at temperatures high enough to relieve the compressive residual hoop stress, but instead failed (or were discovered and removed from service) after they had accumulated sufficient rolling cycles at a cool temperature to return to a state of compressive residual hoop stress.

4.5 Residual Axial Stress

Axial residual stress measurements were made on 10 AAR Class C wheels. Test specimens encompassed at least 3 in in the circumferential dimension and were extracted from the wheels using band-saw cuts. TTCI engineers recorded axial strain readings on two of the wheels before and after extraction of the test specimen to verify that the extraction method did not produce significant changes in residual stress. Six of the wheels failed in service because of VSR, three of the wheels were unfailed service-worn wheels, and one wheel was in the new as-manufactured state with no service loading. The specimens from the three unfailed service-worn wheels were free of subsurface cracks or large defects based on UT results. Table 4 contains additional details about the wheels and the results of the axial residual stress measurements, including the maximum tensile and compressive residual stresses and the radial depth at which the axial

residual stress transitioned from compression to tension. The "Highest Impact Load" values in Table 4 are the largest WILD readings for each wheel for up to 18 months prior to the date the wheel was removed from service.

Residual stress measurements were conducted by using the slitting method. Two strain gages were installed on each wheel section—one on the tread surface and one on the front rim fillet. An incremental slit was cut into the specimen using wire electrical discharge machining (EDM). Wire-cutting EDM is commonly used to minimize residual stresses imparted by the cutting process. The slit was located 2 in from the wheel front rim face and cut through the wheel rim at 0.05-inch radial increments. The released strains were recorded at each incremental cut depth. A finite element model was then used to generate geometry specific coefficients relating the experimentally measured strain to residual stress. Figure 24 shows a wheel specimen after the slit has been cut. The referenced literature contains more detail on this measurement technique (Prime 1999, DeWald, et al. 2004).

Table 4. Details of Wheels and Results from Axial Residual Stress Testing

TTCI Wheel ID	History	Years in Service	Design	Rim Thickness (inch/16)	Highest Impact Load (pounds * 1000)	Max Compression (ksi)	Max Tension (ksi)	Radial Depth of Transition (inch)
14	VSR	7.5	CH36	14	57	-47.7	35.3	0.41
9	VSR	2.1	CH36	23	138	-54.9	21.7	0.42
69	VSR	7.0	CH36	25	69	-57.0	35.1	0.49
30	VSR	1.3	CH36	23	70	-65.5	33.3	0.43
35	VSR	4.1	CH36	18	114	-52.1	60.7	0.54
36	VSR	1.3	H36	27	85	-51.4	37.9	0.45
54	Worn	2.1	CH36	23	79	-55.4	29.0	0.38
41	Worn	3.5	CH36	18	50	-67.7	29.8	0.36
37	Worn	1.3	H36	27	75	-52.2	38.5	0.47
N1	New	0.0	CH36	Nominally 24	N/A	-11.3	2.6	0.56

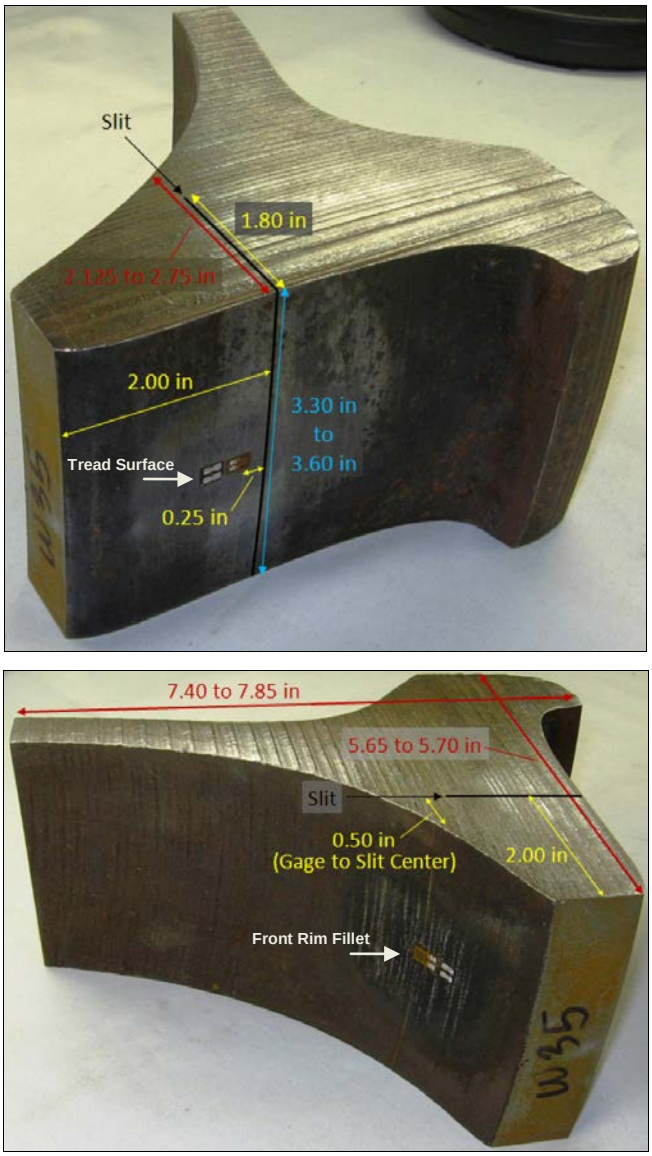

Figure 24. Wheel Specimen after Slitting Operation Showing Typical Dimensions (photos courtesy of Hill Engineering, LLC)

Figure 25 shows the average composite axial residual stress as a function of radial depth for the VSR wheels, the service-worn wheels, and the as-manufactured wheel. A radial depth of 0.0 in indicates the tread surface.

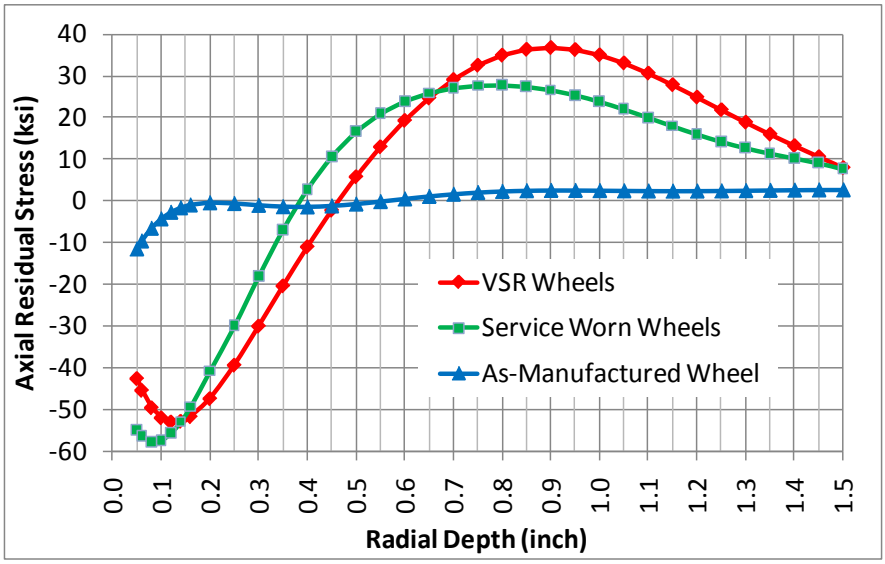

Figure 25. Composite Results of Axial Residual Stress Testing of Class C Wheels

The most striking observation from the results is the overwhelming influence the service load environment has on the axial residual stress in AAR Class C wheels. While the heat treatment during manufacturing imparts a relatively small compressive residual stress near the tread surface, the service load environment produces much larger compressive and tensile axial residual stresses from the plastic deformations associated with rolling contact. The VSR wheels and the service-worn wheels show similar trends—i.e., large compressive residual stress near the tread surface transitioning to large tensile residual stress at approximately 0.4-inch radial depth.

When failed and unfailed parts both show similar results in a laboratory test, there is a tendency to exclude the property under test from consideration as a critical factor in the failure mode. However, the axial residual stresses in AAR Class C wheels should be viewed as a clue to the VSR failure mode. As the inspection results showed, the VSR initiation sites from 35 broken wheels have a median value of 0.17 in radially below the tread surface. This means that a VSR crack need only propagate approximately 0.23 in deeper, radially, from point of maximum stress before entering a tensile residual stress field that would encourage rapid growth. The difference between the VSR wheels analyzed and the unfailed service-worn wheels is the presence of a VSR crack that propagated to the depth of the tensile axial residual stress field.

Wheel-rail contact forces can be increased statically using heavier axle loads or dynamically through impact loads from tread surface discontinuities such as shelling or spalling. Wheel tread damage and increased wheel impact loads are common features of wheels that fail from VSR. Increased wheel-rail contact force not only causes an increase in the magnitude of subsurface stress in wheels, but also increases the radial depth at which the maximum stress occurs. Higher stresses occurring at a radially deeper location could propagate existing cracks (such as from shells or spalls) to radially deeper locations and possibly into the axial tensile residual stress

zone. The farther a crack propagates into the axial tensile residual stress zone, the higher the probability that the crack would continue propagating parallel to the front rim face and form a VSR.

4.6 Section Summary

Microcleanliness tests conducted on 25 VSR wheels and 5 broken flange wheels show that failure of the AAR microcleanliness test is not a prerequisite for VSR or broken flange failure. Twenty-eight of the 30 wheels tested met current AAR microcleanliness standards and the 2 wheels that did not meet current standards were manufactured before those standards were applicable. The microcleanliness of the steel in the wheels tested appears to be typical of many wheels in service today.

The thermal history testing showed at least 5 out of 15 VSR wheels with estimated maximum temperatures that may have exceeded 1,000 °F, yet the residual hoop stress testing showed that all of the wheels were in a state of compressive residual hoop stress. For the wheels that may have been hot, this implies that the wheels failed (or were discovered and removed from service) after they had accumulated sufficient rolling cycles at a cool enough temperature to return to a state of compressive residual hoop stress.

While the heat treatment during manufacturing imparts a relatively small compressive residual stress near the tread surface, the service load environment produces much larger compressive and tensile axial residual stresses from the plastic deformations associated with rolling contact. The VSR wheels and the service-worn wheels show similar trends—i.e., large compressive residual stress near the tread surface transitioning to large tensile residual stress at an approximately 0.4-inch radial depth. This is approximately 0.23 in radially deeper on average than the visually identified VSR initiation location found during inspection, meaning that a crack would only have to propagate a short distance before entering a tensile residual stress field that would accelerate the crack growth.

5. Attempts to Create VSR Cracks under Controlled Conditions

The ability to create a specific failure mode under controlled conditions not only demonstrates understanding of the conditions needed for failures, but also allows for the possibility of parametric testing to better define the relative influence of different conditions. This section describes TTCI's attempts to create a VSR.

5.1 Rolling Load Machine Tests

An existing rolling load machine was modified in an attempt to create a VSR in the laboratory. This machine longitudinally cycles a short piece of rail (approximately 3 ft long) back and forth underneath a stationary wheel. The machine needed modification to allow fine lateral position control for a service-worn wheel and to increase the maximum wheel-rail vertical contact force to 90,000 lb. Figure 26 shows a schematic of the rolling load machine, and Figure 27 is a photograph of the machine.

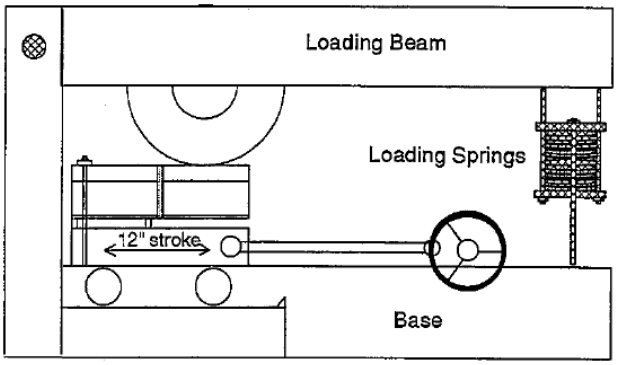

Figure 26. Schematic of TTCI's Rolling Load Machine

Figure 27. TTCI's Rolling Load Machine

A service-worn wheel originally mounted on the same wheelset as a VSR wheel was selected as the first test wheel. Based on UT, this wheel was known to have a large subsurface horizontal crack. The wheel was installed on the test machine so that the field side edge of the horizontal crack was approximately in the center of the contact patch between the wheel and rail. The vertical load was set to 60,000 lb at the beginning of the test. After 4.5 million load cycles, the load was increased by 10,000 lb approximately every million-load cycle until the maximum load rating for the machine was achieved. The test was intended to force the horizontal crack to turn vertically. Instead, the horizontal crack expanded in area early in the test, and then stopped growing until the vertical load was increased. The initial area of the crack was 1.4 in^2 and grew to 3.4 in^2. Crack area was estimated daily by scanning the wheel with a handheld UT device and noting the edges of the horizontal crack compared with a grid overlaid on the wheel with ½-inch grid spacing increments. TTCI believes decreases in the estimated crack area are the result of changes in the tread surface condition during the test that at times provided a suboptimal surface for the contacting ultrasonic probe.

Significant runout of 0.110 in developed on the wheel tread from deformation and wear, forcing the rolling load machine to work harder on every load cycle. After approximately 6.8 million load cycles, the test was stopped because the machine was no longer able to cycle the rail because of the combination of large contact force and radial runout on the wheel. Figure 28 shows the effect of wear and deformation on the transverse wheel profile. Figure 29 shows the crack area and the wheel-rail contact force from this test as a function of the number of load cycles.

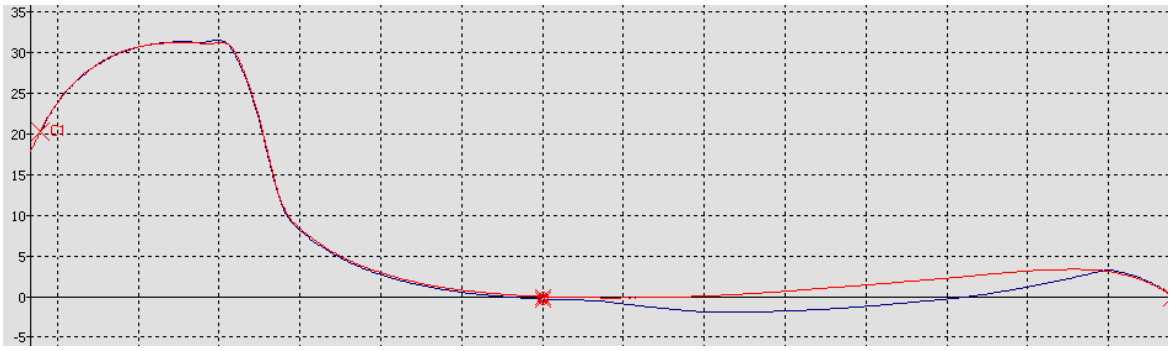

Figure 28. Transverse Wheel Profiles at the Location with Maximum Radial Runout (blue) and at a Circumferential Location that did not Contact the Rail during the Rolling Load Test (Red)

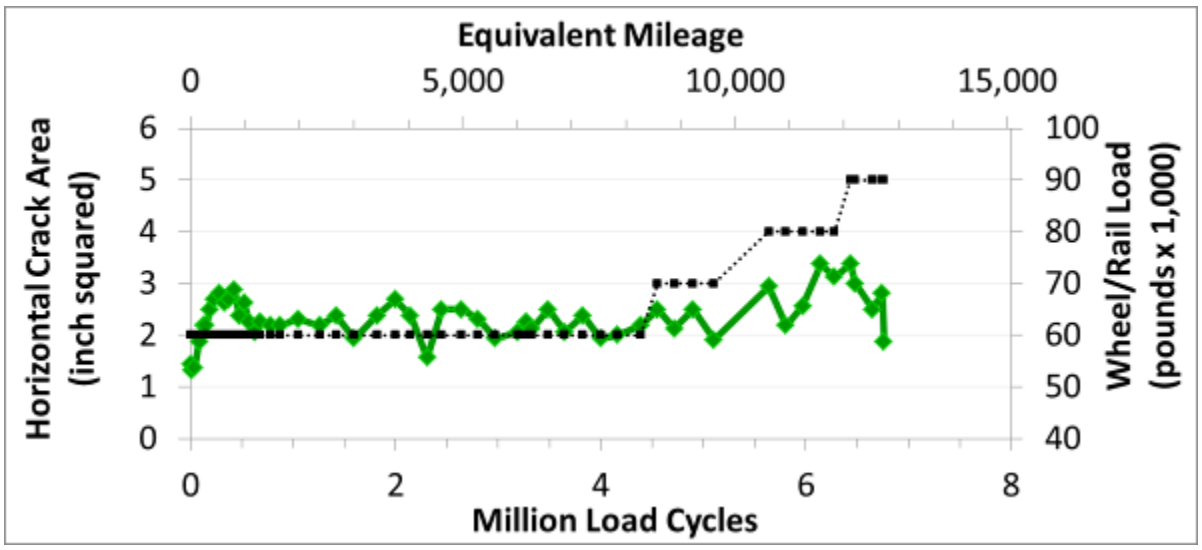

Figure 29. Horizontal Crack Area (Green) and Contact Loads (Black) from the First Rolling Load Test

A second wheel with a 4.3 in^2 preexisting horizontal crack was selected (also originally mounted on the same wheelset as a VSR wheel), and testing was resumed. The vertical load was initially set to 50,000 lb and increased by 10,000 lb approximately every million-load cycle up to the machine maximum. Again, the wheel developed a significant radial runout of 0.120 in from deformation and wear during the test. After 7.4 million load cycles, the machine experienced a failure in one of the support posts, and the test was stopped. The crack area in the wheel did not change appreciably during this test. Figure 30 shows the crack area and the wheel-rail contact force from the second test.

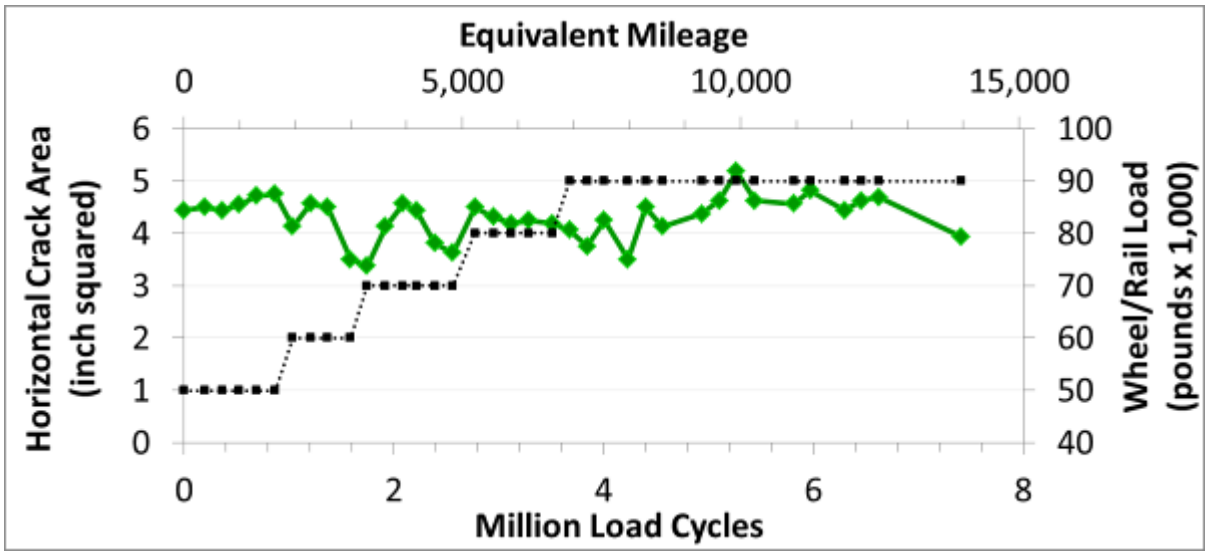

Figure 30. Horizontal Crack Area (Green) and Contact Loads (Black) from the Second Rolling Load Test

Following the tests on the rolling load machine, each wheel was sectioned and the cracks were viewed under a microscope. The horizontal cracks were found to be between 0.08 and 0.20 in below the tread surface with a typical depth of 0.15 in. Multiple short vertical branches stem from the main horizontal cracks. Figure 31 shows the longest vertical branch found, about 350 µm, at the end of a horizontal crack. This vertical branch is linking a number of small inclusions, and numerous other smaller vertical branches can be seen growing toward the tread surface (top of photo) and further into the rim (bottom of photo). Interestingly, the majority of the vertical crack branches found in these two wheels through optical microscopy were on the flange side of the horizontal cracks, even though the wheel-rail contact during the rolling load test was on the field side of the horizontal cracks. This may be an indication that the bending moment generated in the rim by wheel-rail contact is more critical to producing vertical crack branching than localized stresses nearest to the contact patch.

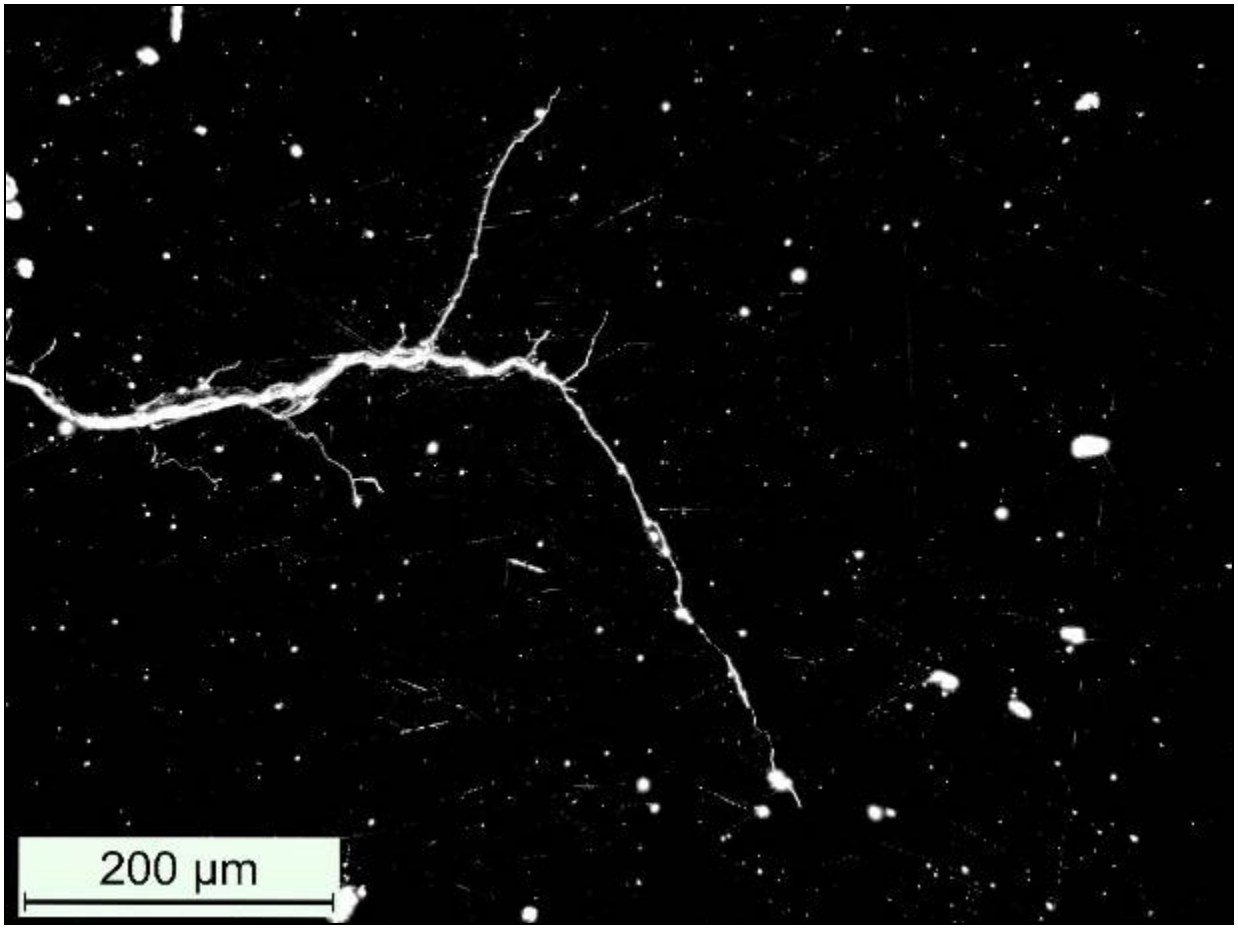

Figure 31. Dark Field Optical Microscopy Shows a Horizontal Crack with Multiple Vertical Branches

As discussed in Section 3, understanding the propagation path of a crack can help define the relative influence of high stress levels and localized material weaknesses. Nonmetallic inclusions act as stress concentrators and tend to solidify at the grain boundaries as ingots solidify and cool. The crack propagation paths of selected cracked specimens from the rolling

load test wheels were further investigated using Norfolk Southern's SEM. The polished samples were etched with a saturated solution of picric acid to show the microstructure, including the boundaries between prior austenite grains. The horizontal cracks and the vertical crack branches examined in the samples removed from the two wheels that failed to develop VSR cracks all showed crack propagation through the middle of grains (transgranular) rather than between prior austenite grain boundaries (intergranular). This is a strong indication that high stress levels were the main driving force in the crack propagation of these two wheels. If the cracks had followed prior austenite grain boundaries, it would have been an indication that material weakness played a large role in the crack development. Figure 32 shows a typical example of a crack in one of the test wheels as viewed through the SEM.

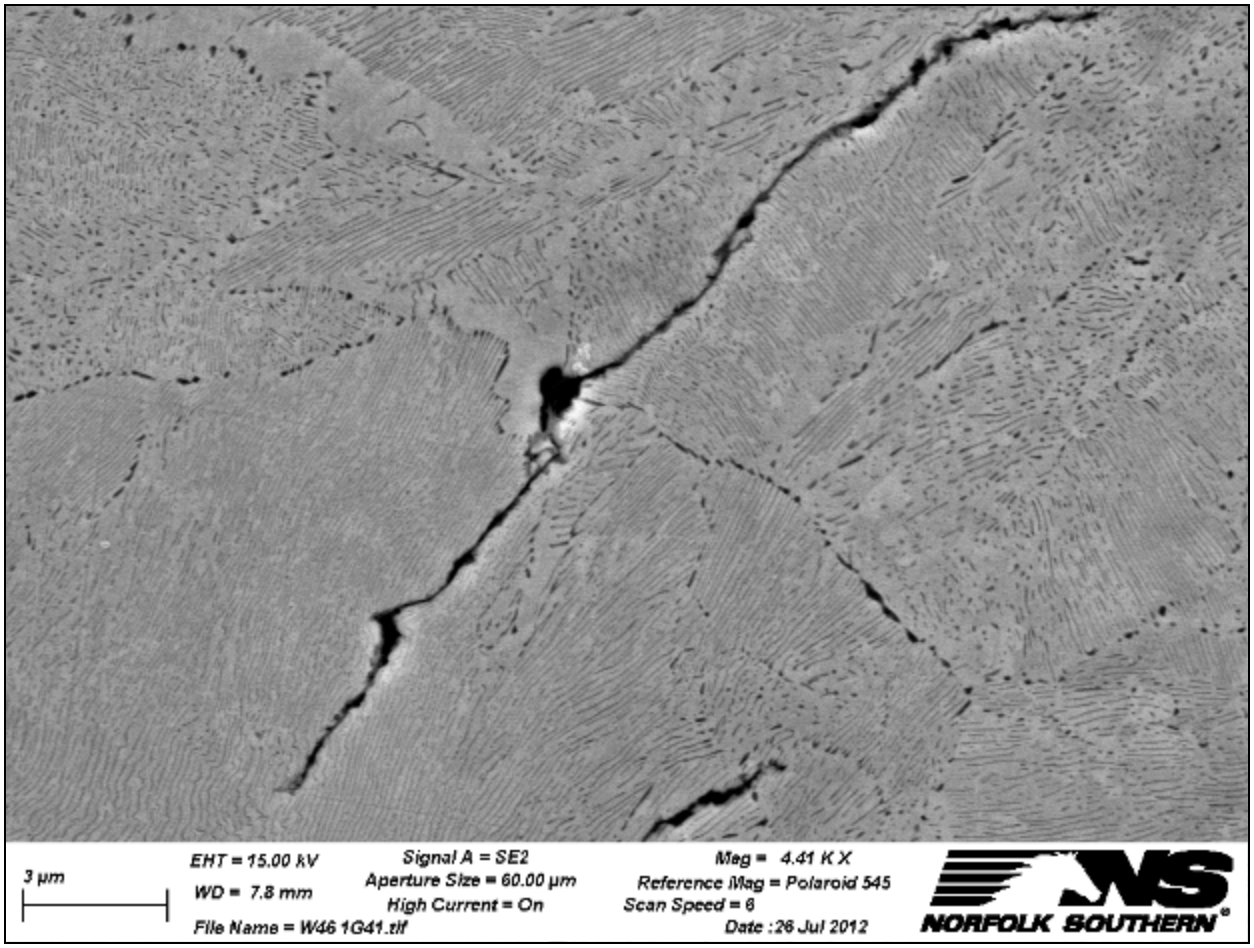

Figure 32. Transgranular Crack Propagation (image courtesy of Norfolk Southern)

The rolling load machine does a good job of representing the wheel-rail contact forces on tangent track, but it is missing a number of characteristics that could be important in producing a vertical crack in a wheel rim. For example, the test was not able to accurately reproduce revenue service impact loads from special trackwork, frictional forces due to curve negotiation, wheel heating from brake applications, or a wet and corrosive environment. Any or all of these factors may play a role in the formation of VSRs. It should be noted that VSRs are an extremely rare event

in terms of ton-miles carried per wheel, and it may take the intersection of many low probability events to produce a VSR, including the presence of a wheel that is unusual in some way. In other words, it is possible that the perfect test would fail to produce a VSR on the majority of wheels. What can be learned from the results of this testing is that cyclic vertical loads far in excess of the standard vertical load are insufficient to produce a VSR in service-worn wheels with large preexisting horizontal cracks.

5.2 Section Summary

Two service-worn wheels with large naturally occurring subsurface horizontal cracks were cycled on a rolling load test machine at wheel-rail forces as high as 90,000 lb in an attempt to create a VSR wheel under controlled conditions. In each case, the test machine failed after about 7 million load cycles, and the test was stopped. Neither test wheel developed a VSR crack, although post-test destructive evaluation revealed short vertical crack branches in both wheels. The horizontal cracks were found at a typical radial depth of 0.15 in, which is nearly the same radial depth as the VSR crack origins identified during the wheel inspections. SEM analysis showed that the cracks propagated in a transgranular fashion, indicating that material weakness was not a primary cause for the crack development in these two wheels.

6. Mitigation

Increasingly, broken wheel rims are due to VSR failures, with an associated decline in the number of shattered rims. This section describes the successful mitigation efforts already in place for shattered rims and discusses potential options for VSR.

6.1 Shattered Rim

The root causes of shattered rims have been studied and agreed upon in the literature. They include nonmetallic inclusions in forged wheels and voids in cast wheels combined with large impact loads. Based on these findings, the AAR has established and/or tightened criteria in the areas of UT, wheel impact loads, and microcleanliness testing. AAR repair records show that the number of wheels removed from service for shattered rim has been on a steady decline for at least a decade. The AAR has already recognized and implemented mitigation efforts for shattered rims.

6.2 VSR and Broken Flange

Without increased understanding of why and how VSR failures occur, it would be premature to recommend mitigation strategies.

The literature offers a theory for the VSR and broken flange failure process and work conducted under this project generally supports the theory (i.e., shells or spalls on the wheel tread provide a source of cracks and impact loads). The cracks propagate through an area of residual axial compressive stress to an area of residual axial tensile stress where crack growth accelerates and a portion of the wheel rim breaks free. However, the means by which a crack propagates deep enough into the rim to reach the zone of tensile residual stress is not clear, as illustrated by unsuccessful attempts to create a VSR under controlled conditions.

Over the past decade, no clear trend has been evident in AAR repair records regarding the number of wheels removed from service for cracked or broken rim. Microcleanliness testing of VSR wheels and reports of UT records from one wheel manufacturer have not shown enough reason to suspect wheel cleanliness as a major factor in VSR formation. Restricting the levels of allowable impact loads produced by wheels may have had a small positive influence in reducing the number of VSRs, but the effect is not nearly as evident as in the case of shattered rims.

Several vendors are developing or improving upon existing wayside automated detection methods for cracked wheels. However, it is not clear how many miles a VSR wheel travels between the time a detectable condition is present and failure occurs. The influence of other parameters such as load magnitude, ambient temperature, and lateral position of the contact patch on the wheel tread (dependent on wheel-rail profiles and track geometry) are also unknown. Additional study on this matter is critical to helping solve the VSR problem.

7. Conclusion

Broken rims are the leading cause of wheel-related accidents, and they are increasing as a percentage of all equipment-related accidents. The 3-year-average count of FRA reportable accidents attributed to broken rims has increased slightly in recent years from 16.0 (2004 to 2006) to 19.3 (2009 to 2011) (FRA 2012). Broken rim wheel failures generally fall into one of two categories: shattered rim or VSR.

The root causes of shattered rims have been studied and agreed upon in the literature. Effective mitigation efforts for shattered rims have been recognized and implemented by the AAR, including tighter UT limits on allowable defects, tighter microcleanliness limits, and the establishment of a maximum impact load criteria. Shattered rims have been on the decline for the past decade, recently accounting for less than 0.01 percent of wheel removals in the AAR car repair billing database (AAR 2012).

Shattered rims and VSRs have some distinct differences including the following:

- Shattered rims are on the decline while accidents due to VSRs are on the rise.
- Shattered rims are reported throughout the world while VSRs are reported only in North America.
- The shattered rim failure mode is well understood by the industry and has been replicated under controlled conditions, while the VSR failure mode is less well understood and attempts to replicate this failure mode in the laboratory have not been successful.

VSRs are thought to be the result of tread damage on the wheel surface in the form of shell or spall that initiates cracking in the rim and produces impact loads when it contacts the rail (Dick, et al. 2008; Lonsdale and Oliver 2011). If the crack propagates vertically to an area of tensile residual stress in the wheel rim, further crack growth is encouraged until a portion of the rim breaks free from the wheel.

Inspections of 29 VSR wheels and 6 broken flange wheels showed a broad range of wheels, including cast and forged wheels, reprofiled wheels and wheels in their first life cycle, and wheels removed from many different car types including cars with gross rail load ratings of 110, 100, and 70 tons. Only a few of the VSR wheels had hollow worn profiles and the flange height, flange thickness, and rim thickness values were considered in the normal expected range. A VSR origin location was identified for each wheel, and radial depths of these origins were all found in a tight band ranging from 0.10 to 0.25 in below the tread surface with a median value of 0.17 in. Shells were noted on the tread surface in close proximity to the origin point for 29 of the 35 wheels. If an 11,000-kip day removal criterion was used along with the current 90,000-pound impact load limit, 24 of the 35 broken wheels would have been condemnable at the time of their removal based on WILD readings. UT revealed horizontal cracks in 27 of the 35 broken wheels and 18 of the 35 mate wheels. A common feature found on many of the broken wheels was a horizontal separation between two visually distinct layers in the wheel rim typically occurring no more than 0.25 in below the tread surface.

Microcleanliness tests conducted on 25 VSR wheels and 5 broken flange wheels show that failure of the AAR microcleanliness test is not a prerequisite for VSR or broken flange failure. Twenty-eight of the 30 wheels tested met current AAR microcleanliness standards and the 2

wheels that did not meet current standards were manufactured before those standards were applicable. The microcleanliness of the steel in the wheels tested appears to be typical of many wheels in service today.

The residual stress patterns in the axial direction of VSR wheels and the service-worn wheels show similar trends—i.e., large compressive residual stress near the tread surface transitioning to large tensile residual stress at an approximately 0.4-inch radial depth. This is approximately 0.23 in radially deeper on average than the visually identified VSR initiation location found during inspection, meaning that a crack would only have to propagate a short distance before entering a tensile residual stress field that would accelerate the crack growth.

Two service-worn wheels with large naturally occurring subsurface horizontal cracks were cycled on a rolling load test machine at wheel-rail forces as high as 90,000 lb in an attempt to create a VSR wheel under controlled conditions. In each case, the test machine failed after about 7 million load cycles, and the test was stopped. Neither test wheel developed a VSR crack, although post-test destructive evaluation revealed short vertical crack branches in both wheels. The horizontal cracks were found at a typical radial depth of 0.15 in, which is nearly the same radial depth as the VSR crack origins identified during the wheel inspections. SEM analysis showed that the cracks propagated in a transgranular fashion, indicating that material weakness was not a primary cause for the crack development in these two wheels.

Additional research is needed for VSRs. Adding or modifying specifications for newly manufactured wheels and/or reprofiled wheels cannot be justified at this time based on the current research results. Wayside automated detection methods for cracked wheels could potentially provide some reduction in VSRs; however, many factors still need to be addressed, including the following:

- The relationship between the number of load cycles and the VSR crack size.
- The influence on this relationship of parameters such as load magnitude, impact loading, ambient temperature, and lateral position of the contact patch on the wheel tread.

8. Acknowledgments

A group of wheel experts provided assistance with the visual inspections and provided suggestions for harvesting the microcleanliness test samples from the failed wheels. The group included Huseyin Guzel and Glenn Bowen from BNSF Railway, John Oliver and Cameron Lonsdale from Griffin Wheel Company, Steve Dedmon from Standard Steel, LLC, and Dan Stone from Hunter Holiday Consulting.

Steve Dedmon of Standard Steel, LLC examined all of the microstructure photographs for the thermal history analysis and provided his best estimate of the highest temperature reached by each wheel sample.

Norfolk Southern Railway provided the use of their SEM for analysis of specimens.

Daniel Szablewski of TTCI provided direction for the metallurgical analysis of the wheels and captured images using Norfork Southern's SEM. Greg Giebel and Ken Trujillo of TTCI provided daily UT support during the rolling load machine testing and hand-mapped each VSR wheel and mate. Sirius Roybal of TTCI carefully maintained the rolling load machine and monitored the testing throughout a total of approximately 14 million load cycles.

9. References

Ameen, P. "Ultrasonic Inspection of Reprofiled Wheels at Wheel Shops," Circular Letter C-9467, Washington, DC, May 2002.

Association of American Railroads. *Manual of Standards and Recommended Practices,* Section G, Part II, Wheel and Axle (Shop) Manual, RP-631, Washington, DC, 2012.

Association of American Railroads. *Manual of Standards and Recommended Practices,* Section G, Wheels and Axles, M-107/M-208, Washington, DC, 2011.

Association of American Railroads, Car Repair Billing Database, data queried November 2012.

Beretta, S. Donzella, G., Roberti, R., and Ghidini A. "Deep Shelling in Railway Wheels," *Proceedings of the 13th International Wheelset Congress*, Rome, Italy, September 2001.

Berge, S. "Shattered rim fracture research," *Proceedings of 2000 Brenco Rail Conference,* LaQuinta, California, October 19–20, 2000.

Berge, S. "Wheel Shelling Study Group," Presentation to the BNSF Wheel Shelling Study Group, Topeka, Kansas, 2001.

Dahlman, G. and Lonsdale, C., "Strategies to Prevent Heavy Haul Wheel Failures," *Proc. Of International Heavy Haul Association Conference,* Dallas, TX, May 5–6, 2003.

Dedmon, S., "Microstructural Evaluation of Wheel Steel Using Simulated Service Thermal Loads," RTDF2009-18010, *Proceedings of ASME Rail Transportation Division Fall Conference*, Ft. Worth, TX, October 20–21, 2009.

DeWald, A.T., et al. "Assessment of tensile residual stress mitigation in Alloy 22 welds due to laser peening," *Journal of Engineering Materials and Technology*, 126(4), 465–473, 2004.

Dick, M., Iwand, H., McConnell, D., Magner, J., and Snyder, T. "Characterization of Vertical Split Rim Failures," Presentation to BNSF Wheel Shelling and Failure Study Group, Topeka, Kansas, 2008.

Federal Railroad Administration, data queried from safety database in November 2012 (http://safetydata.fra.dot.gov/OfficeofSafety/default.aspx)

Galbraith, J., Ames, G., and Leister, S., "Consistent and Repeatable Property and Residual Stress Control in Forged and Heat Treated Railway Wheels," JRC2011-56089, *Proc. Of ASME and Joint Rail Conference,* Pueblo, CO, March 16–18, 2011.

Kristan, J., Stone, D., and Elkins, J. "Effect of Wheel Loading on the Occurrence of Vertical Split Rim Wheel Failures," *Proc. IMECE2004-59049, ASME International Mechanical Engineering Congress & Exposition*, 2004.

Lonsdale, C. and Oliver, J. "Further Research into Wheel Rim Axial Residual Stress and Vertical Split Rim Failures," *Proceedings of ASME/ASCE/IEEE 2012 Joint Rail Conference,* JRC2012-74010, Philadelphia, PA, 2012.

Lonsdale, C. and Oliver, J. “Wheel Rim Axial Residual Stress and a Proposed Mechanism for Vertical Split Rim Formation,” *Proceedings of ASME Rail Transportation Division Fall Conference*, RTDF2011-67024, Minneapolis, MN, 2011.

Lonsdale, C., Rusin, T., and Hay, T. “Research to Understand the Effects of Wheel Impact Loads on Wheel Stress Levels,” JRC2009-63026 *Proc. ASME Joint Rail Conference*, Pueblo, CO, March 3–5, 2009.

Lunden, R. “Cracks in Railway Wheels under Rolling Contact Load,” *Proceedings of the 10th International Wheelset Congress*, Australia, 1992, pp. 163–168.

Marais, J. “Wheel Failures on Heavy Haul Freight Wheels Due to Subsurface Defects,” *Proceedings of the 12th International Wheelset Congress*, Quingdao, China, 1998, pp. 306–314.

Pilch, J. “Heat Treatment of a Railroad Wheel,” 2008 International ANSYS Conference, Pittsburg, PA, 2008.

Prime, M.B. “Residual stress measurement by successive extension of a slot: The crack compliance method.” *Applied Mechanics Reviews*, 1999, 52, 75–96.

Rajkumar, B. and Stone, D. “Wheel Failure Mechanisms of Railroad Cars,” AAR Report R-679, Pueblo, CO, 1987.

Stahura, T. “Implementation of Revision to M-107/208 Ultrasonic Test Requirements,” Circular Letter C-9019, Washington, DC, June 1999.

Stahura, T. “Implementation of Revision to Section G, Specification M-107/208, Paragraphs 8 and 9 (Incorporate Microcleanliness Specifications),” Circular Letter C-9714, Washington, DC, October 2003.

Stahura, T. “Subject: Implementation of Advanced Technology Safety Initiative (ATSI) Rule Changes—Opportunistic Repair: Rule 41.A.2.l,” Circular Letter C-10132, Washington, DC, June 2005.

Stahura, T. “Implementation of Changes: Revision of MSRP, Section G, Specification M-107/M-208, Paragraph 18.4.5.1, Ultrasonic Inspection Rejection,” Circular letter C-10275, Washington, DC, March 2006.

Stahura, T. “Implementation of Revisions to AAR Manual of Standards and Recommended Practices (MSRP) Section G, Specification M-107/M-208, Rule 9.3.3,” Circular Letter C-10483, Washington, DC, April 2007.

Stone, D. and Dahlman, G. “The Effect of Discontinuity Size on the Initiation of Shattered Rim Defects,” ASME Rail Transportation Division Volume 19, 2000, pp. 7–14.

Stone, D., Lonsdale, C., and Kalay, S. “Effect of Wheel Impact Loading on Shattered Rims,” *Proceedings of the 13th International Wheelset Congress*, Rome, Italy, September 17–21, 2001.

Stone, D., Tournay, H., and Cummings, S. “Broken Wheel Inspections,” *Technology Digest* TD-09-008, Association of American Railroads, Transportation Technology Center, Inc., Pueblo, CO, March 2008.

Sura, V. and Mahadevan, S. “Shattered Rim Failure Modeling in Railroad Wheels,” RTDF2010-42028, *Proc. ASME Rail Transportation Division Fall Technical Conference*, Roanoke, VA, October 12–13, 2010.

Sura, V. and Mahadevan, S. “Vertical Split Rim Failure Analysis in Railroad Wheels,” JRC2010-36024, *Proc. Joint Rail Conference*, Urbana, IL, April 27–29, 2010.

Wang, K. “The Probabilistic Study of Heat Treatment Process for Railroad Wheels Using ANSYS/PDS,*” 2006 International ANSYS Conference*, Pittsburg, PA, 2006.

Appendix A.
Inspection Wheel Details

TTCI ID	Failure Type	Mate ID	Car Type	Loc	Class	Wh Type	Wh Size	Mfg Date	Rim Thick (1/16 inch)	Flg Hgt (in)	Flg Thck (in)	Hollow (mm)	Defect Depth (inch)
1	VSR	51	S350	L1	C	J	33	Jan-06	24	1.2	1.3	0	0.16
2	VSR	59	C114	R2	C	CJ	36	Oct-03	22	1.1	1.2	0	0.19
3	VSR	58	T108	R3	C	CH	36	Jul-93	20	1.2	1.2	0	0.17
4	VSR	60	T107	L2	C	H	36	Mar-91	18	1.3	1.2	0	0.16
5	Brk Flg	64	S110	L3	C	CJ	33	Aug-05	18	1.3	1.4	1.57	0.15
6	VSR	62	J302	L2	C	CJ	36	Oct-03	24	1.2	1.3	0	0.10
7	VSR	63	F451	L3	C	CJ	36	Jan-04	21	1.2	1	0	0.21
8	VSR	55	C114	R3	C	CH	36	Mar-06	23	1.2	1.3	0	0.10
9	VSR	54	J303	R4	C	CH	36	May-06	24	1.2	1.3	0	0.20
10	VSR	53	S367	LZ	C	CB	38	Dec-04	22	1.3	1.2	1.72	0.24
11	VSR	52	C614	L3	C	CJ	36	Sep-02	21	1.1	1.1	0	0.17
12	VSR	56	A405	L3	C	J	36	Aug-91	19	1.1	1.2	0	0.18
13	VSR	57	A606	L1	C	CH	36	May-99	25	1.3	1.2	0	0.14
14	VSR	50	C113	L1	C	CH	36	Aug-01	14	1.1	1	0	0.16
15	VSR	49	C113	L3	C	CJ	36	Nov-93	17	1.3	1.3	2.51	0.21
16	Brk Flg	61	S615	R4	C	CJ	33	May-05	18	1.4	1.3	2.74	0.24
17	Brk Flg	46	F483	R4	C	CH	36	Oct-00	16	1.1	1.3	0	0.12
18	VSR	48	C113	L3	C	CH	36	Jan-07	18	1.1	1.3	0	0.11
19	VSR	47	C113	L1	C	CJ	36	Mar-04	23	1.1	1.2	0	0.16
21	VSR	20	C113	R3	C	CH	36	Oct-96	17	1.3	1.3	0	0.23
22	Brk Flg	23	K341	L3	C	CH	36	Oct-03	16	1.1	1.2	0	0.17
24	VSR	25	J311	L2	C	CH	36	Jun-08	27	1.1	1.4	0	0.25
27	VSR	26	C112	R2	C	CH	36	Feb-02	17	1.1	1.3	0	0.18
28	VSR	29	A606	R1	C	CH	36	May-00	17	1.1	1.2	0	0.14
30	VSR	31	J311	R1	C	CH	36	Oct-08	23	1.2	1.3	0	0.16
32	VSR	33	C113	L2	C	CJ	36	May-02	31	1.3	1.3	0	0.21
35	VSR	34	K341	R1	C	CH	36	Dec-05	18	1	1.2	0.47	0.19
36	VSR	37	A606	R1	C	H	36	Jul-08	27	1.2	1.3	0	0.24
38	VSR	39		L1	C	CH	36	Oct-06	18	1.1	1.1	0	0.18
40	VSR	41	C112	L4	C	CH	36	Oct-04	18	1.1	1.2	0	0.22
43	VSR	42	A405	L1	C	CH	36	Feb-94	20	1.1	1.3	0	0.21
45	VSR	44	K341	L2	C	CH	36	Apr-05	22	1.5	1	6.12	0.17
67	Brk Flg	65	H351	R2	C	CH	36	Apr-95	19	1.2	1.3	0	0.14
69	VSR	66	F443	R1	C	CH	36	Jun-01	25	1.2	1.3	0	0.15
70	Brk Flg	68	J302	L2	C	CH	36	Aug-95	18	1.3	1.1	1.42	0.18

TTCI ID	Highest Impact (kips)	Highest Dynamic (kips)	Peak Kip Days	Dynamic Kip Days	Locking Plate	Wheel Age (years)	Tread Age (years)	Turned Wheel?	Rim rollover	Shells at VSR init?	Comments
1	103.3		4509	2947		2.0			N	Y	
2	153.8	118.7	1756	986	Oct-03	5.1	5.1	New	N	Near	
3	82.2	64.8	26666	15949	Jan-00	15.6	9.1	Turned	N	Y	
4	45.5	12.5	0	0		18.0			N	Y	
5	98.9	92.2	17495	14058	Oct-05	2.8	2.7	New	N	Near	
6	92.5	60.2	43801	26750	Mar-06	5.8	3.4	Turned	N	Y	
7	65.5	26.1	0	0	Jun-08	5.2	0.8	Turned	N	No	
8	96.1	56.6	1004	583		2.1			N	Y	
9	138.2	104.5	138	105	May-06	0.7	0.7	New	N	No	
10	111.7	73.2	6060	3752	Dec-04	2.3	2.3	New	N	Y	Broken Plate
11	66.0	32.3	11299	5528	May-08	6.9	1.2	Turned	N	No	
12	102.2	93.1	27007	14007		17.5			N	Y	
13	107.9	95.6	44594	28214	Jul-99	9.9	9.7	New	Y	Y	
14	56.9	25.3	0	0	Feb-06	7.5	3.0	Turned	N	No	
15	123.6	86.9	13281	7456		15.4			Y	Near	
16	125.0	103.5	30317	22501	May-05	1.9	1.9	New	Y	Y	
17	70.7	35.9	71	36	Mar-08	8.5	1.1	Turned	Y	Near	
18	176.0	141.2	278	199	May-08	2.3	1.0	Turned	N	No	
19	94.9	58.4	4843	2650	Mar-07	5.0	2.0	Turned	Y	Y	
21	93.3	60.5	27535	15905	Aug-01	12.4	7.5	Turned	N	No	
22	53.2	13.2	0	0	Jan-08	5.5	1.2	Turned	Y	Y	
24	72.7	35.3	1001	486	Jun-08	0.8	0.8	New	N	Y	
27	67.5	35.8	35385	18744	Jun-06	7.4	3.1	Turned	Y	Y	
28	74.1	42.5	2694	1556	Oct-07	9.0	1.6	Turned	N	Y	
30	70.4	33.6	2784	1273	Oct-08	1.3	1.3	New	N	Y	
32	81.5	50.0	55360	32315	May-02	7.6	7.6	New	Y	Y	
35	114.2	82.0	9256	5278	Feb-08	4.1	1.9	Turned	Y	Y	
36	85.1	50.0	21088	12206	Nov-08	1.3	1.0	New	N	Near	
38	104.7	65.2	5111	2775	Sep-08	3.2	1.3	Turned	Y	Y	
40	40.3	23.2	0	0	May-06	5.1	3.5	Turned	N	Y	
43	87.7	57.2	15128	9763	Oct-06	15.5	2.8	Turned	N	Y	Intact
45	68.5	29.9	0	0	Apr-05	3.9	3.9	New	N	Near	Brake Head Wear
67	75.9	43.9	16209	8485	Sep-04	13.8	4.4	Turned	Y	Y	
69	68.7	33.1	5675	2732	Jul-01	7.0	7.0	New	N	Y	Derail damage
70	86.1	51.2	17739	9113	Sep-98	13.7	10.6	Turned	Y	Y	

Appendix B.
Fatigue Crack Growth Rate Test Results

Westmoreland Mechanical Testing & Research, Inc.

dadN vs. ΔK Graph

Phone: (724) 537-3131

Customer : TTCI
WMT&R Report : 0-73531
WMT&R Quote : QN101417
Material : Steel 0.7%C

Frequency : 10 Hertz
Temperature : Room
Environment : Lab Air

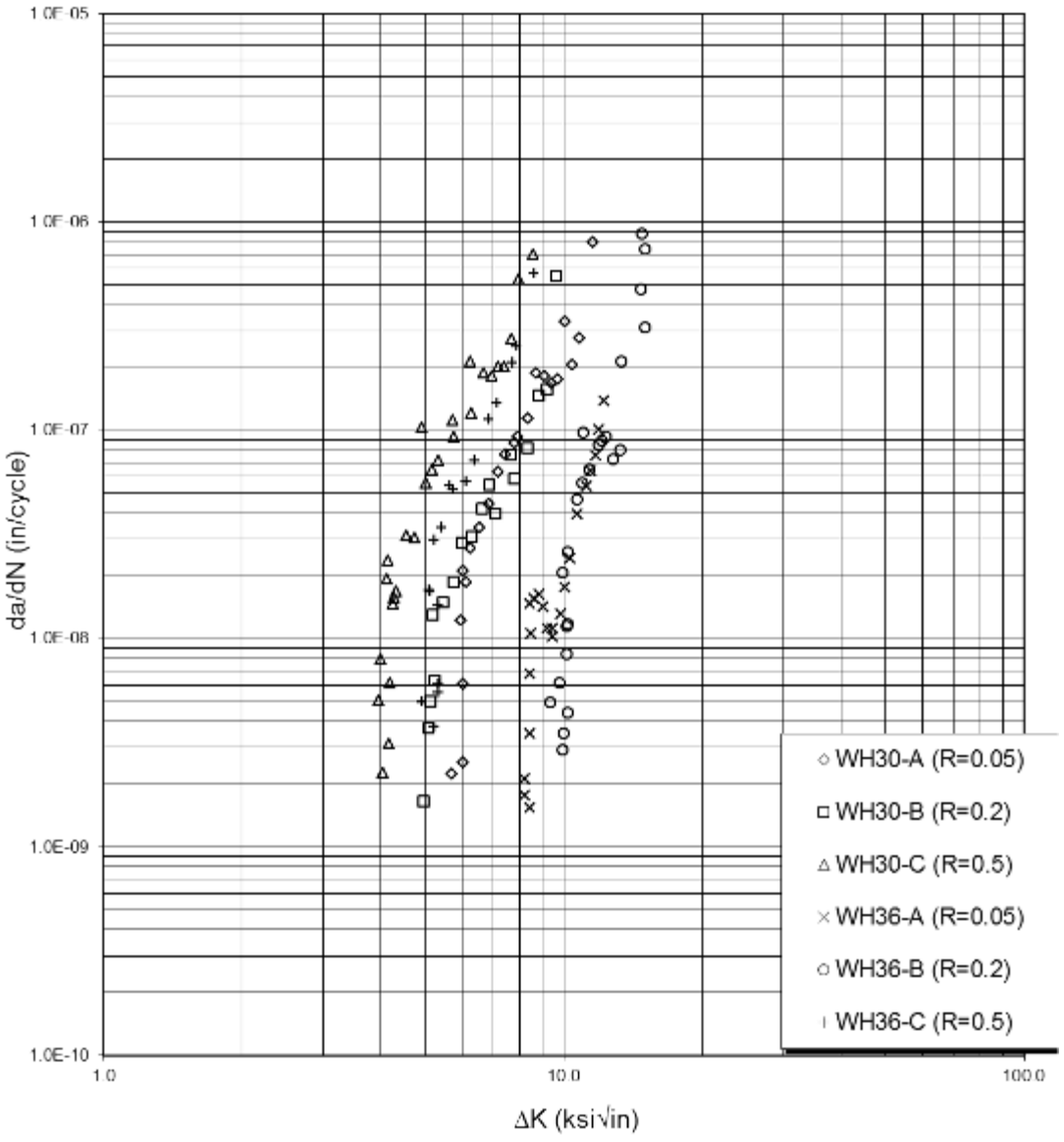

Abbreviations and Acronyms

AAR	Association of American Railroads
ASTM	American Society for Testing and Materials
DAC	Distance Amplitude Correction
EDM	electrical discharge machining
FRA	Federal Railroad Administration
SEM	scanning electron microscope
TIR	total indicator runout
TTCI	Transportation Technology Center, Inc.
UT	ultrasonic testing
VSR	vertical split rim
WILD	wheel impact load detector
WMC	Why Made Code